Thermal process enhancement of HNCPCM filled heat sink: Effect of hybrid nanoparticles ratio and shape

Adeel Arshad[a,*], Mark Jabbal[a], Hamza Faraji[b], Muhammad Anser Bashir[c], Pouyan Talebizadehsardari[d], Yuying Yan[a,e,*]

[a]*Fluids & Thermal Engineering (FLUTE) Research Group, Faculty of Engineering, University of Nottingham, Nottingham NG7 2RD, UK*
[b]*Physics Department, LPMMAT Laboratory, Faculty of Sciences Ain Chock, Hassan II University, Casablanca, Morocco*
[c]*Department of Mechanical Engineering, Mirpur University of Science & Technology (MUST), Mirpur 10250, AJK, Pakistan*
[d]*Department of Mechanical and Aerospace Engineering, Institute of Energy Futures, Brunel University London, Uxbridge, Middlesex UB8 3PH, UK*
[e]*Research Centre for Fluids and Thermal Engineering, University of Nottingham Ningbo China, Ningbo 315100, China*

Abstract

The present study based on the numerical investigation of a hybrid nanocomposite phase change material (HNCPCM) filled heat sink for passive cooling of electronic devices. The combination of graphene oxide (GO) and silver (Ag) hybrid nanoparticles are added inside the RT-28HC to enhance thermal performance. The volume fraction ratios of Ag:GO are varied from 0:0, 0:4, 1:3, 2:2, 3:1 and 4:0. Four different shape factor values of 3.7, 4.9, 5.7 and 16.1 of Ag-GO are varied. The transient simulations are carried out to solve the governing equations using the finite volume method scheme. The results depicted that employing HNCPCM has better heat transfer enhancement compared to the pure PCM because of the addition of nanoparticles. The results showed that adding the Ag-GO inside the RT-28HC improved the thermal conductivity and uniformity in the melting process compared to the RT-28HC based heat sink. With the addition of Ag-GO, melting time of HNCPCM filled heat sink is reduced and heat transfer rate in increased. The optimum ratio of 1:3 of Ag:GO nanoparticles and shape factor value of 16.1 show the higher thermal conductivity of 0.348 W/m.K, 12.93% reduction in melting time, 8.65% enhancement in heat storage capacity and rate of heat transfer.

Keywords: Hybrid nanocomposite phase change material; Graphene oxide (GO); Silver (Ag); Heat sink; Electronics cooling

*Correspondence authors

Email addresses: adeel.arshad@nottingham.ac.uk, adeel_kirmani@hotmail.com (Adeel Arshad), yuying.yan@nottingham.ac.uk (Yuying Yan)

Nomenclature

Abbreviations

Ag	Silver
Cu	Copper
FVM	Finite volume method
HS	Heat sink
TM	Thermal management
HNCPCM	Hybrid nanocomposite phase change material
PCM	Phase change material
PRESTO	PREssure STaggering Option
QUICK	Quadratic Upstream Interpolation for Convective Kinematics
SIMPLE	Semi-Implicit Pressure-Linked Equation
GO	Graphene oxide

Symbols

A_m	Mushy zone
B	Boltzman constant (J/K)
ρc_p	Volumetric heat capacity $(J/m^3.K)$
g	Gravitational acceleration (m/s^2)
H	Height (mm)
Q	Heat storage capacity (J)
q	heat storage density (J/kg)
k	Thermal conductivity $(W/m.K)$
L	Latent heat of fusion $(J/kg.K)$
m	Mass (kg)
p	Pressure (Pa)
$\dot{Q}$	Rate of heat transfer (W)
$\dot{q}$	Rate of heat transfer density (W/kg)

S	Source term in momentum equation
sf	Shape factor (m)
T	Temperature (K)
t	Time (sec)
u	Velocity component in $x-$axis (m/s)
v	Velocity component in $y-$axis (m/s)
W	Width (mm)
c_p	Specific heat capacity $(J/kg.K)$
ΔH	Fractional latent-heat $(J/kg.K)$
$2D$	Two dimensional

Greek letters

φ	Volume fraction
μ	Viscosity (Pa.s)
β	Thermal expansion coefficient (1/K)
f_l, λ	Liquid fraction
χ	Volume fraction ratio

Subscripts

HS	Heat sink
hs	Heat source
ini	Initial
l	Liquidus
m	Melting
$hncpcm$	Hybrid nanocomposite phase change material
np	Nanoparticles
ref	Reference
x	$x-$axis
y	$y-$axis

1. Introduction

Over the last two decades, a remarkable and revolutionary advancement has been achieved in development of the portable electronic devices in term of miniaturization and faster performance of smart applications with higher power density. Because of this compactness and smart features, electronic circuitry causes to increase the internal heat generation results in the temperature of the critical components increases beyond the critical limits. Therefore, this demands a reliable and effective thermal management (TM) technology for high performance and faster processing portable electronic devices [1, 2]. Since, it has been argued that temperature rise is the key factor almost 55% in deterioration of electronic devices [3]. Compared to the active cooling technologies which include the air or fluids flowing through the either heat pipe, heat sink or microchannels [4, 5, 6, 7, 8], the passive cooling technologies especially based on phase change materials (PCMs) have proven remarkable thermal performance with a *zero-noise*, *zero-power* and longer-term reliability [9]. Obviously, active cooling solutions provide the higher amount of heat transfer rate, however it requires the higher value of energy consumption due to the fan or pump operation, also these generate noise as well [10, 11, 12].

In this context, a passive TM technology consists of PCM and heat sink can exhibits a vital and promising role to reduce the temperature below the critical limit and extend the operation time and functional performance of electronic device. Since, the PCMs have a great potential to absorb/release the excessive heat while heating/cooling process because of higher heat storage density. However, they possess the low thermal conductivity especially organic PCMs [13]. Various strategies have been proposed to enhance the thermal conductivity of the PCM such as metallic fins [14, 15, 16, 17, 18, 19, 20, 21], metallic foams [22, 23, 24, 25], and nanoparticles [26, 27, 28, 29, 30, 31] as thermal conductivity enhancers (TCEs) and micro/nano-encapsulation of PCMs [13, 32, 33, 34, 35]. Qu et al. [22] conducted the numerical study for passive thermal management of high-power Li-ion battery using porous metal-foam with PCM. The results attributed the enhancement of conduction heat transfer because of addition of metal-foam. Ren et al. [31, 36] carried out a comprehensive study with nanoparticles and metal-foam added PCM in heat pipe and studied the melting process by varying the porosity and pore size of metal-foam and volume fraction of nanoparticles. The authors found the addition of nanoparticles and metal-foam combination improved the enhancement in PCM melting. Arshad et al. [19, 20, 21, 37] conducted the numerical and experimental studies to explore the fin thickness of finned heat sink at

3

constant volume fraction of 9% by different PCMs, volumetric fractions of PCM and different power levels. The results reported that 3 mm fin thickness had the better thermal performance by lowering the average heat sink temperature. Arshad et al. [25] conducted a experimental study using CuO coated metal-foam/PCM embedded heat sink of varying metal-foam thickness, PCM volumetric fractions and power level. The results showed that composite of metal-foam/PCM based heat sink improved the heat transfer enhancement and a filling thickness of 0.5 CuO coated metal-foam PCM filled heat sink revealed the best thermal cooling performance.

Although, the insertion of metallic fins and foams show a great improvement in thermal conductivity as well as heat transfer enhancement, however, there are some limitations which need to be overcome. The metal fins and foams cause to loss the capacity of stored latent-heat and increase the overall weight of the heat sink and manufacturing cost. Thus, these limitations can be minimized by dispersing the nanoparticles inside the PCMs to improve its thermal conductivity and uniformity in melting process. However, the thermal energy storage capacity of PCMs decreases with the addition of nanoparticles. In consequence of this, many researchers have revealed the effect of adding nanoparticles inside the PCM based heat sink and/or rectangular or square enclosure [26, 38, 39, 40, 41]. For instance, Farsani et al. [38] numerically studied the melting phenomenon of Al_2O_3 nanoparticles dispersed PCM in a square cavity by varying the Rayleigh number and volume fraction. The authors observed the three regimes of melting process. Firstly, initial melting was due the heat conduction, later was buoyancy driven heat convection, and lastly again it was the heat conduction. Dhaidan et al. [42] carried out an experimental and numerical study using a composite of CuO/n-octadecane in a square cavity under a constant heat flux. Authors explored the effects of nanoparticles loading, Rayleigh number and subcooling. They found that melting interface and liquid-fraction were improved with increase of CuO volume fraction. With the increase of Rayleigh number, the melting process of PCM was expedited. Colla et al. [39] studied the thermophysical and heat transfer performance of nano-PCM in a square cavity. The results showed that nano-PCM delayed the melting process compare to the pure PCM. Bondareva et al. [26] investigated the heat transfer performance of nanoparticles added PCM filled cooling system and found the increase in melting rate with increase of nanoparticles concentration. Authors reported that melting phenomenon accelerated by adding nanoparticles initially due to heat conduction in solid and liquid PCM layers. Faraji et al. [40, 41] reported the computational studies based on horizontal and inclined rectan-

gular enclosures filled with Cu nanoparticles and PCM. The authors found that addition of Cu nanoparticles of varying volume fractions reduced the heat source temperature.

The development of nanoparticles dispersed PCM showed that mixing metallic or metallic-oxide nanoparticles improved the thermophysical properties of pure PCM. In addition, uniform heating/cooling and enhanced heat transfer rates were obtained during melting and solidification processes [43] The enhanced attribute in thermophysical properties and heat transfer performance is because of the higher thermal conductivity of nanoparticles. In continuous development of nanoparticles dispersed PCMs with more than one nanoparticles, with different thermophysical properties, have proved the more better dispersion uniformity, thermal and chemical stability and heat transfer distribution [44, 45, 46]. For instance, Ghalambaz et al. [44] conducted a numerical study using hybrid nanoparticles of Ag-MgO dispersed in octadecane filled in a square cavity. They found that hybrid nanoparticles composed of Ag-MgO showed the best fusion performance compared to the pure octadecane and MgO-octadecane. Arshad et al. [45, 46] developed the metallic-oxide and carbon additives based mono and hybrid nanoparticles dispersed nanocomposite PCMs. The authors found the better thermal stability and higher thermal conductivity by using hybrid nanoparticles of Al_2O_3+CuO and GNP+MWCNT nanoparticles. Safaei et al. [47] conducted a experimental study to synthesize the GO based NCPCM with different volume fraction of GO and found that GO/paraffin showed the 25% productivity improvement compared the pure paraffin. Further, Safaei et al. [48] investigated the thermal and electrical performance of photovoltaic/thermal system using PCM and nanofluid. The authors used MWCNTs and water/ethylene glycol (50:50) nanofluid and paraffin as a PCM. They found the around 20% electrical enhancement and 130% thermal enhancement of the system. Alizadeh et al. [49] conducted a numerical study based of TiO_2-Cu nanoparticles dispersed in pure PCM filled in a Y-shaped fins latent heat thermal energy storage system. The authors studied the solidification process. It was found that suspension of TiO_2-Cu nanoparticles with fin enhanced the solidification rate because of the improved thermal conductivity. Hosseinzadeh et al. [50] carried out the numerical study using Al_2O_3-GO hybrid nanoparticles with PCM in a snowflake structure and studied the solidification process of latent heat thermal energy storage system. The authors found that 0.04 volume fraction of Al_2O_3-GO nanoparticles improved the solidification rate of 24.1%. Recently, Faraji et al. [51] conducted a numerically study using single and hybrid nanoparticles dispersed PCM in a rectangular enclosure. They used the Al_2O_3, ZnO, CuO and Cu nanoparticles and n-eicosane as a PCM. The authors

5

found that using hybrid nanoparticles of 1%-Al$_2$O$_3$ and 3%-Cu showed a 5.77% reduction in base temperature compared to the pure n-eicosane.

From aforementioned literature, it can be revealed that most of the studies explored the phase change phenomenon of single nanoparticles dispersed PCMs. Thus, the current numerical study explores the melting phenomenon and heat transfer performance of hybrid nanocomposite phase change material (HNCPCM) filled heat sink for passive cooling thermal performance. The graphene oxide (GO) and silver (Ag) nanoparticles are selected and a total constant volume fraction of 4.0% is fixed and individual volume fraction of Ag and GO is varied from 0.0% to 4.0% with an increment of 1.0%. The optimum ratio of GO and Ag is explored and constant power level is applied at the heat sink base. The thermal process enhancement and melting phenomenon of HNCPCM filled heat sink is evaluated through different thermal performance evaluation indicators such melting time, heat storage capacity, heat storage density, rate of heat transfer, and rate of heat transfer density.

2. Geometric and Mathematical description

2.1. Physical model

The computational domain used for current study is shown in Fig. 1 which consists on a HNCPCM based heat sink. A two-dimensional rectangular heat sink is considered equal to the dimensions of normal heat sink technology for passive cooling of electronic devices proposed in previous experimental studies [18, 52]. The height and width of the heat sink, made of copper, are selected as $H = 25$ mm and $W = 70$ mm, respectively, and a mimic heat generation source, (q'''), with sizes of $l = 50$ mm and $t = 2$ mm is located at the base of the heat sink representing the internal heat generating source of an electronic device. A constant input power level of 5 W is applied at the heat sink base. The sides walls of the heat sinks are considered as adiabatic except top surface which undergoes with natural convection effects. The internal domain of the heat sink with dimensions of width ($w = 60$ mm) and height ($h = 20$ mm) is filled with different volume fractions of silver (Ag) and graphene oxide (GO) hybrid nanoparticles. The volume fraction ratio (χ) of Ag:GO hybrid nanoparticles is varied from 0:0, 0:4, 1:3, 2:2, 3:1 and 4:0. The total φ of Ag-GO is fixed constant of 4%, and individual φ of Ag and GO is varied from 0% to 4% with an increment of 1% of φ. The thermophysical properties of RT–28HC, which is used PCM, Ag and GO nanoparticles are listed in Table 1. The current system is designed to investigate passive

6

thermal performance and melting phenomenon of HNCPCM based heat sink of portable electronic components.
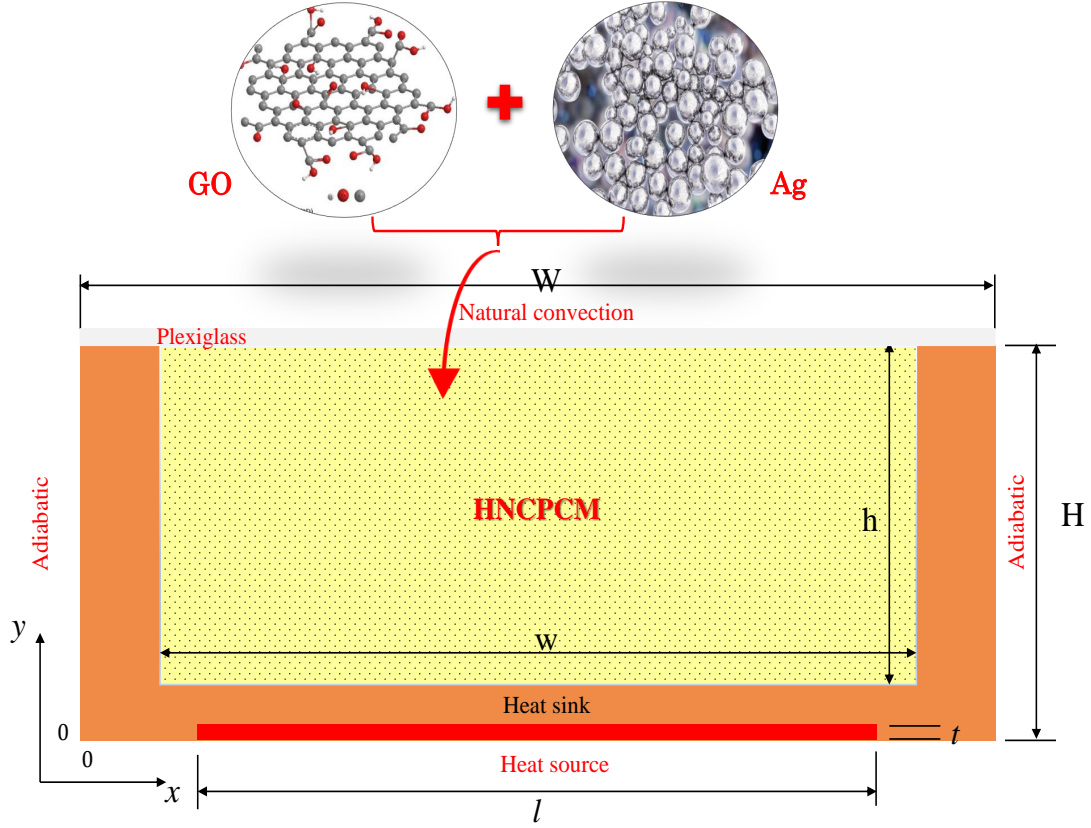
Figure 1: *Schematic diagram of the physical domain used in current study.*

2.2. Numerical model

To simulate the phase change heat transfer and melting process of HNCPCM based heat sink, the enthalpy-porosity model is adopted in which the porosity is fixed equal to the liquid-fraction of each grid. The heat conduction flow is considered for the heat sink whereas, conduction and convection heat flow are considered for HNCPCM which is the mixture of Ag-GO and RT-28HC. For solving the continuity, momentum and energy equations of a HNCPCM filled heat sink, shown in Fig. 1, the following assumptions are considered for present study:

- The constant thermophysical properties of heat sink, PCM and hybrid nanoparticles are considered.

- A colloid suspension is taken for HNCPCM which exhibits as a Newtonian fluid. The flow regime is two-dimensional, laminar, transient, and incompressible of liquid HNCPCM and viscous dissipations are considered negligible.

7

Table 1: Thermophysical properties of PCM, heat sink and nanoparticles [50, 53, 54, 55].

Physical properties	RT-28HC	Cu	GO	Ag
T_m (K)	301.15	-	-	-
T_s (K)	300.15	-	-	-
T_l (K)	302.15	-	-	-
L (J/kg)	250,000	-	-	-
μ (Pa.s)	0.00256			
k (W/m.K)	0.2	400	5000	429
c_p (J/kg.K)	2000	380	717	235
ρ (kg/m^3)	880 (solid) 770 (liquid)	8920	1800	10500
β (1/K)	0.0006	-	-	-

- A homogeneous without agglomeration suspension is assumed by dispersing the hybrid nanoparticles.

- The PCM and hybrid nanoparticles are in local thermal equilibrium and there is no–slip between them.

- Negligible volume change is assumed of HNCPCM during phase–change process.

- The heat sink is considered as solid–state with homogeneous and isotropic properties and thermal conduction heat transfer exists.

- The initial temperature of heat sink and HNCPCM are the same temperature.

- No–slip boundary conditions are considered for velocities at the boundaries.

- The Boussinesq approximation is used to model the buoyancy driven force under natural convection as $\rho = \rho_m/\beta(T - T_m) + 1$, where $T_m = (T_s + T_l)/2$.

Thus, the following governing equations are defined to model the HNCPCM flow motion and temperature variation inside the heat sink are governed by the standard Navier–Stokes and energy equations:

Continuiy:

$$\frac{\partial u}{\partial x} + \frac{\partial v}{\partial y} = 0 \tag{1}$$

Momentum in x–direction:

$$\rho_{hncpcm}\left(\frac{\partial u}{\partial t} + u\frac{\partial u}{\partial x} + v\frac{\partial u}{\partial y}\right) = -\frac{\partial p}{\partial x} + \mu_{hncpcm}\left(\frac{\partial^2 u}{\partial x^2} + \frac{\partial^2 u}{\partial y^2}\right) + S_x \tag{2}$$

8

Momentum in y–direction:

$$\rho_{hncpcm} \left(\frac{\partial v}{\partial t} + u\frac{\partial v}{\partial x} + v\frac{\partial v}{\partial y} \right) = -\frac{\partial p}{\partial y} + \mu_{hncpcm} \left(\frac{\partial^2 v}{\partial x^2} + \frac{\partial^2 v}{\partial y^2} \right) +$$

$$(\rho\beta)_{hncpcm}g(T - T_{ref}) + S_y \quad (3)$$

where:

$$S_x = A_m \frac{(1-\lambda)^2}{(\lambda^3 - 0.001)}.u \qquad S_y = A_m \frac{(1-\lambda)^2}{(\lambda^3 - 0.001)}.v \quad (4)$$

where, the ρ_{hncpcm}, μ_{hncpcm}, β_{hncpcm} are the density, dynamic viscosity, and thermal expansion coefficient of the HNCPCM, respectively; p and g are the pressure and gravitational acceleration, respectively. The S_x and S_y are source terms, defined by Carman–Kozeny relation for flow in porous media, in x and y directions, respectively. The source terms represent a gradual reduction in velocities from a finite value in liquid to zero in solid, over the computational cell that undergoes the phase–change phenomenon. This means that each cell behaves like a porous media whose porosity is equal to liquid–fraction. The A_m is the mush–zone constant which reflecting the morphology of melting front. The value of A_m is chosen of 10^5 kg/m^{3}s present study [28, 37, 38]. Additionally, λ is the liquid–fraction during the phase–change in temperature interval of $T_s < T < T_l$ and it varies between 0 (solid) to 1 (liquid), which is defined as:

$$\lambda = \begin{cases} 0 & \text{if} \quad T < T_s \\ \frac{T - T_s}{T_l - T_s} & \text{if} \quad T_s \leq T \leq T_l \\ 1 & \text{if} \quad T < T_l \end{cases} \quad (5)$$

Energy (liquid–phase):

$$(\rho c_p)_{hncpcm} \left(\frac{\partial T}{\partial t} + u\frac{\partial T}{\partial x} + v\frac{\partial T}{\partial y} \right) = k_{hncpcm} \left(\frac{\partial^2 T}{\partial x^2} + \frac{\partial^2 T}{\partial y^2} \right) - \frac{\partial(\rho\Delta H)_{hncpcm}}{\partial t} \quad (6)$$

Energy (soild–phase):

$$(\rho c_p)_{hncpcm} \left(\frac{\partial T}{\partial t} \right) = k_{hncpcm} \left(\frac{\partial^2 T}{\partial x^2} + \frac{\partial^2 T}{\partial y^2} \right) \quad (7)$$

where, $(\rho c_p)_{hncpcm}$ is the volumetric heat capacity and ΔH_{hncpcm} is the fractional latent–heat of the HNCPCM which is expressed in terms of latent–heat of fusion L_{hncpcm} as follows:

$$\Delta H_{hncpcm} = \lambda L_{hncpcm} \tag{8}$$

where:

$$\Delta H_{hncpcm} = \begin{cases} 0 & \text{if} \quad T < T_m \\ \lambda L_{hncpcm} & \text{if} \quad T \geq T_m \end{cases} \tag{9}$$

Since, the only heat conduction heat transfer mode is considered for heat sink and heat source. Thus, the corresponding governing equations can be written as follow:

Energy (heat sink):

$$(\rho c_p)_{HS} \left(\frac{\partial T}{\partial t} \right) = k_{HS} \left(\frac{\partial^2 T}{\partial x^2} + \frac{\partial^2 T}{\partial y^2} \right) \tag{10}$$

Energy (heat source):

$$(\rho c_p)_{hs} \left(\frac{\partial T}{\partial t} \right) = k_{hs} \left(\frac{\partial^2 T}{\partial x^2} + \frac{\partial^2 T}{\partial y^2} \right) + q''' \tag{11}$$

where, $(\rho c_p)_{HS}$, k_{HS} $(\rho c_p)_{hs}$, and k_{hs} are the volumetric heat capacity and thermal conductivities of heat sink and heat source, respectively.

2.3. Thermophysical properties of HCNPCM

The thermophysical properties of HCNPCM are varied with the addition of hybrid nanoparticles of different volume fraction ratios. The thermophysical properties of RT-28HC, used as a pure PCM, Ag and GO nanoparticles are listed in Table 1. The effective properties such as density (ρ_{hncpcm}), specific heat capacity ($c_{p_{hncpcm}}$), latent–heat of fusion (L_{hncpcm}), thermal expansion coefficient (β_{hncpcm}), dynamics viscosity (μ_{hncpcm}), and thermal conductivity (k_{hncpcm}) HCNPCMs are calculated using theoretical models of mixtures as follows [51]:

$$\rho_{hncpcm} = \varphi_2 \rho_{np_2} + \left[(1 - \varphi_2) \left\{ \varphi_1 \rho_{np_1} + (1 - \varphi_1) \rho_{pcm} \right\} \right] \tag{12}$$

$$(\rho c_p)_{hncpcm} = \varphi_2 (\rho c_p)_{np_2} + \left[(1 - \varphi_2) \left\{ \varphi_1 (\rho c_p)_{np_1} + (1 - \varphi_1)(\rho c_p)_{pcm} \right\} \right] \tag{13}$$

10

$$(\rho L)_{hncpcm} = (1 - \varphi_1)(1 - \varphi_2)(\rho L)_{pcm} \tag{14}$$

$$(\rho\beta)_{hncpcm} = \varphi_2(\rho\beta)_{np_2} + \left[(1 - \varphi_2)\left\{\varphi_1(\rho c_p)_{np_1} + (1 - \varphi_1)(\rho\beta)_{pcm}\right\}\right] \tag{15}$$

$$\mu_{hncpcm} = \frac{\mu_{pcm}}{(1 - \varphi_1)^{2.5}(1 - \varphi_2)^{2.5}} \tag{16}$$

$$\frac{k_{hncpcm}}{k_{ncpcm}} = \frac{k_{np_2} + (sf - 1)k_{ncpcm} - (sf - 1)(k_{ncpcm} - k_{np_2})\varphi_2}{k_{np_2} + (sf - 1)k_{ncpcm} + (k_{ncpcm} - k_{np_2})\varphi_2} \tag{17}$$

where:

$$\frac{k_{ncpcm}}{k_{pcm}} = \frac{k_{np_1} + (sf - 1)k_{pcm} - (sf - 1)(k_{pcm} - k_{np_1})\varphi_1}{k_{np_1} + (sf - 1)k_{pcm} + (k_{pcm} - k_{np_1})\varphi_1} \tag{18}$$

In above Eqs. 12–18, φ_1 and φ_2 represent the volume fractions of nanoparticles of type 1 and nanoparticles of type 2, respectively. The subscripts $hncpcm$, np, pcm, np_1 and np_2 refer to the HCNPCM, nanoparticles, PCM, nanoparticles of type 1 and nanoparticles of type 2, respectively.

2.4. Initial and boundary conditions

The initial and boundary conditions applied in current study are labelled in Fig. 1. The side walls of the heat sink are defined as an adiabatic boundary condition except the top surface which is undergoes the natural convection effect. Following are the initial and boundary conditions applied in this work to solve the governing equations as follows:

1. Initial conditions

$t = 0$, $T(0) = T_{ini} = 296.15$ K, $f_l = 0$

2. Boundary conditions

• No–slip condition at walls: $u = v = 0$

• Adiabatic walls:

$-k\left.\frac{\partial T}{\partial x}\right|_{x=0,W} = 0$ Along vertical walls

$-k\left.\frac{\partial T}{\partial y}\right|_{\substack{x=0-10,60-70 \\ y=0}} = 0$ At bottom surface

• Natural convection:

$-k\left.\frac{\partial T}{\partial y}\right|_{y=H} = h(T - T_\infty)$ At Top surface

11

205 • Volumetric heat generation provided from heat source:

206 $$-k \left. \frac{\partial T}{\partial y} \right|_{\substack{x=10-60 \\ y=0-2}} = q'''$$

207 *2.5. Performance evaluation parameters*

208 To estimate the thermal performance of HNCPCM based heat sink, four different perfor-
209 mance evaluation parameters such as heat storage capacity (Q), heat storage density (q), rate
210 of heat transfer $(\dot{Q})$, and rate of heat transfer density $(\dot{q})$ along with the total melting time
211 (t_{melt}). The total Q is defined as the total thermal energy storage capacity during the pre–
212 sensible heating, latent–heat of fusion, and post–sensible heating of HNCPCM. Whereas, q
213 indicates the total thermal energy storage capacity per unit mass of the HNCPCM. The Q
214 and q can be defined by Equations 19 and 20, respectively, as follows:

$$Q = m_{hncpcm} \left(\int_{solid} c_{p_{hncpcm}} dT + \lambda L_{hncpcm} + \int_{liquid} c_{p_{hncpcm}} dT \right)$$
$$\approx m_{hncpcm}[c_{p_{hncpcm}}(T_m - T_i) + \lambda L_{hncpcm} + c_{p_{hncpcm}}(T_m - T_f)] \quad (19)$$

215 and

$$q = \frac{Q}{m_{hncpcm}} = \frac{m_{hncpcm} \left(\int_{solid} c_{p_{hncpcm}} dT + \lambda L_{hncpcm} + \int_{liquid} c_{p_{hncpcm}} dT \right)}{m_{hncpcm}}$$
$$\approx \frac{m_{hncpcm}[c_{p_{hncpcm}}(T_m - T_i) + \lambda L_{hncpcm} + c_{p_{hncpcm}}(T_m - T_f)]}{m_{hncpcm}} \quad (20)$$

216 Since, the Q and q can only evaluate the storage capacity of HNCPCM based heat
217 sink relative to the mass of HNCPCM. However, there is no relationship of total t_{melt} of
218 HNCPCM with Q and q. Thus, the overall thermal performance of heat sink cannot be
219 evaluate only with Q and q. Therefore, the effect of t_{melt}, m_{hncpcm}, and Q are combined
220 together to define the rate of heat transfer $(\dot{Q})$ and rate of heat transfer density $(\dot{q})$. The $\dot{Q}$
221 indicates the total thermal energy storage capacity per unit melting time and $\dot{q}$ is defined as
222 total thermal energy storage capacity per unit melting time and per unit mass of HNCPCM,
223 by Equations 21 and 22, respectively, as follows:

12

$$\dot{Q} = \frac{Q}{t_{melt}} = \frac{m_{hncpcm} \left(\int_{solid} c_{p_{hncpcm}} dT + \lambda L_{hncpcm} + \int_{liquid} c_{p_{hncpcm}} dT \right)}{t_{melt}}$$
$$\approx \frac{m_{hncpcm}[c_{p_{hncpcm}}(T_m - T_i) + \lambda L_{hncpcm} + c_{p_{hncpcm}}(T_m - T_f)]}{t_{melt}} \quad (21)$$

and

$$\dot{q} = \frac{Q}{t_{melt}.m_{hncpcm}} = \frac{m_{hncpcm} \left(\int_{solid} c_{p_{hncpcm}} dT + \lambda L_{hncpcm} + \int_{liquid} c_{p_{hncpcm}} dT \right)}{t_{melt}.m_{hncpcm}}$$
$$\approx \frac{m_{hncpcm}[c_{p_{hncpcm}}(T_m - T_i) + \lambda L_{hncpcm} + c_{p_{hncpcm}}(T_m - T_f)]}{t_{melt}.m_{hncpcm}} \quad (22)$$

2.6. Numerical procedure and model validation

The governing equations used in current study are solved by ANSYS–FLUENT 19.1. The melting/solidification model is applied for the phase transition of HNCPCM. The double precision is set to discretize the governing equations of continuity, momentum and energy. The PRESSURE–BASED method is selected which is recommended for incompressible flow with high–order Quadratic Upstream Interpolation for Convective Kinematics (QUICK) differencing scheme presented by Leonard [56] to enhance the accuracy of the numerical method. The Semi-Implicit Pressure-Linked Equation (SIMPLE) algorithm was adopted for pressure–velocity coupling by Patanker [57]. The PRESTO (PREssure STaggering Option) scheme was adopted for pressure correction equation. The gravitational effect is also considered and second–order upwind difference scheme is selected to discretize convective terms in momentum and energy equations. The under-relaxation factors for pressure, velocity, energy and liquid-fraction are set to 0.3, 0.3, 0.8 and 0.5, respectively. The convergence criteria are set to 10^{-4}, 10^{-6} and 10^{-8} for continuity, momentum and energy equations, respectively.

The grid independence test is also carried out using different gird size of 43753, 48305, 54087 and 60796 to avoid its effects on numerical accuracy. The results of melting time and total energy of PCM are summarized in Table 2. The maximum deviation in melting time and total energy is obtained of 0.38% and 0.06% between the elements size of 48305 and 54087, respectively. Thus, the grid with the size of 54087 elements is selected for further simulation. Three different time-steps of 0.05, 0.1 and 0.2 s are varied for mesh size of 54087

13

Table 2: Grid independence analysis.

Number of elements	Melting Time (s)	Deviation (%)	Total energy (kJ/kg)	Deviation (%)
43753	1290	0.00	242.47	0.00
48305	1300	0.78	242.34	0.05
54087	1295	0.38	242.49	0.06
60796	1295	0.00	242.39	0.04

elements and no significance variation is observed. The reason is that PCM upfront velocity and thermal front movement are low, reflecting a low Peclet number and Courant number situation. Therefore, the mesh-size and time-step are 54096 elements and 0.1s, respectively, considered are set in current study.

The numerical results obtained in current study are validated with experimental results carried out using a empty heat sink filled with PCM at $\varphi = 0.0\%$. The RT–35HC is selected as a PCM with melting temperature of 35 °C and a input power level of 5 W is applied at the base of heat sink. The results of average heat sink temperature of numericals study are compared with experimental results, shown in Fig. 2. An acceptable agreement is achieved between the experimental results and the present study. A few discrepancies are observed before the melting and later in phase–change phase which are due to achieving perfectly adiabatic boundary conditions while experimentation and presence impurities in RT–35HC compared with the ideal thermophysical properties provided in numerical study.

The current numerical results of nanoparticles dispersed PCM are validated with previous study by Mahdi and Nsofore [58]. The authors used the horizontal triple-tube thermal energy heat storage unit using RT-82 and Al_2O_3 nanoparticles. A 2% volume fraction of Al_2O_3 nanoparticles is dispersed into the RT-82 and 90 °C is set at inner and outer tubes. The results of the melting process were presented in [58] and compared to the current numerical results. An excellent agreement is obtained with [58], as shown in Fig. 3.

Too further validate the current numerical model, the present numerical results are compared with the experimental results reported by Dhaidan et al. [42]. A melting process of n-octadecane as PCM filled in a square cavity is compared with current numerical results, as shown in Fig. 4. A plexiglass made square cavity with dimensions of $25.4 \times 25.4 \times 25.4$ mm^3 and Rayleigh number of 2.79×10^8 are employed for validation. It can be seen that a reasonable and good agreement between the experimental and numerical results of present study is achieved.
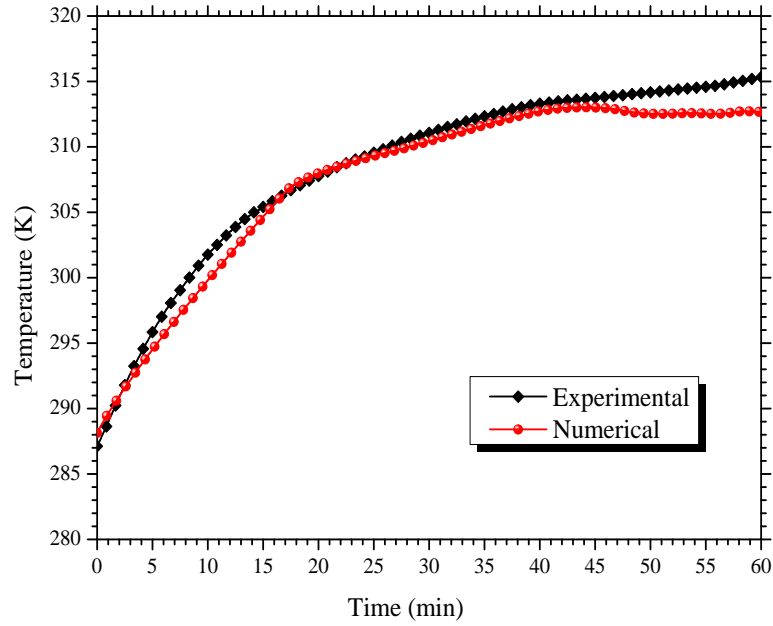
Figure 2: *Validation of present study with experimental results of an empty heat sink filled with PCM at $\varphi = 0.0\%$.*
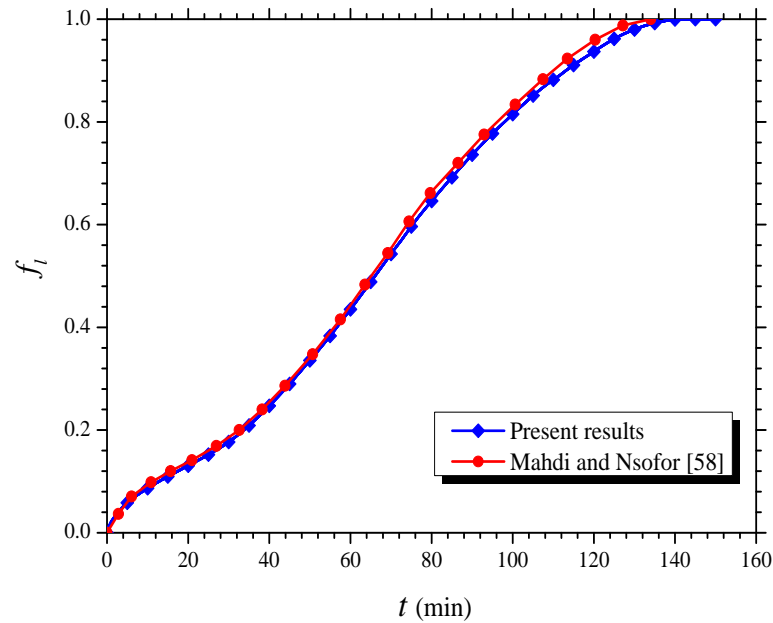
Figure 3: *Validation of present results of nanoparticles/PCM simulation compared with Mahdi and Nsofor at $\varphi = 2.0\%$ [58].*

3. Results and discussion

3.1. Evaluation of isotherms contours

The evolution of isotherms contours of a heat sink filled with HNCPCM at $\chi = 0{:}0$ and $\chi = 1{:}3$ of Ag:GO hybrid nanoparticles is shown at different times in Figure 5. At 300 s, the evolution of isotherms shows that the temperature at the surface of the heat sink is more higher compared to other regions. The present behaviour is essentially due to

15
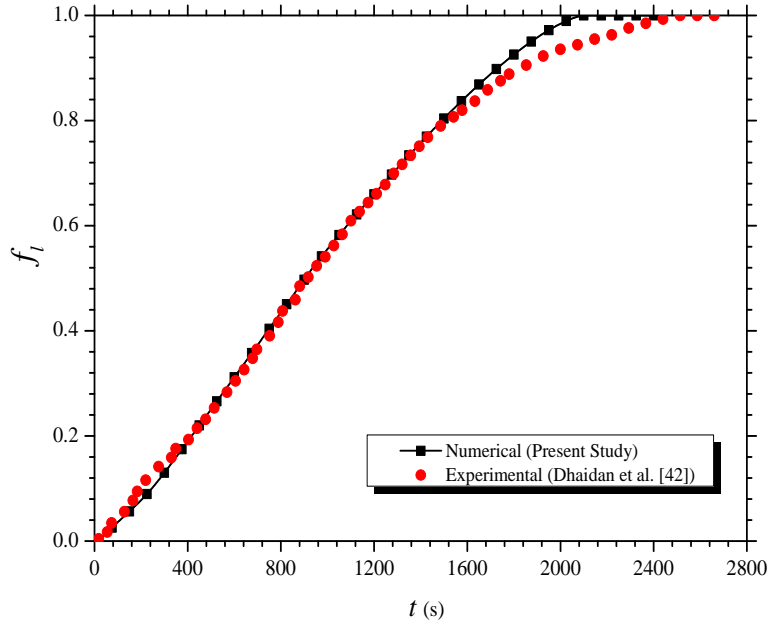
Figure 4: *Validation of present results with experimental results of Dhaidan et al. [42] $\varphi = 0.0\%$.*

the prevailing heat transfer mode, which is purely conductive. This is observed even at the PCM-heat sink interfaces under the effect of the high thermal gradient. The insertion of the hybrid nanoparticles shows a clear ability to lower the temperature of the heat sink and uniform the temperature distribution in the liquid and solid zones of the HNCPCM. At this stage the effect of natural convection is still small or negligible compared to conduction due to the formation of very small right and left circulating patterns at the side walls of heat sink. Moreover, the uniform vortices of isotherms contours at the bottom of the heat sink during melting which are because of the buoyancy force effects developed by the temperature gradient across heat sink base and gravitational force.

Over time, and especially in the plateau region defined by the instants 600 s, 900 s and 1200 s, the liquid HNCPCM region widens and the melting front advances. The number of plume structures decreases over time and the flow structure becomes more complicated and complex. The insertion of hybrid nanoparticles into the PCM always shows its ability to cool the electronic component. In fact, by advancing the melting front, the volume of the liquid HNCPCM increases by increasing the temperature gradient between the electronic component (heat source) and the melting front (heat sink) and subsequently the effect of the buoyancy force. Indeed, the addition of hybrid nanoparticles improve the heat transfer rate and influence the flow of the liquid HNCPCM over the electronic component. The heat transfer mode that prevails in the plateau region is natural convection. This is proven by

16

the increase in the size of the plume structures and their deformation. The increase in size and deformation of vortices are because of the growing role of the convection heat transfer in melt zone. Under the effect of natural convection, the cold HNCPCM moves downward under the gravity effect while pushing the hot HNCPCM to move towards the melting front under the effect of buoyancy force. This movement results in HNCPCM circulation currents for better cooling of the electronic component. Furthermore, it can be observed that the insertion of the hybrid nanoparticles within the base PCM accelerates the melting process and increases the size of the liquid region compared to the PCM alone.

At 1500 s, the observation that can be reported is the complete melting of the HNCPCM and the remainder of a fairly small mass of the solid PCM in the case of a PCM alone without insertion of the hybrid nanoparticles. This behaviour is mainly related to the contribution of both conduction and natural convection in this stage. This accelerates the melting of the PCM in case of the insertion of hybrid nanoparticles due to the new contribution of conduction. The temperature reported in the case of a PCM alone is lower than that recorded for an HNCPCM based heat sink which is because of the lower latent-heat storage capacity and higher thermal conductivity of HNCPCM by the addition of Ag-GO hybrid nanoparticles. More closely, the higher temperature zones at the upper part of the heat sink can be observed compared to the central part of which show that HNCPCM melting is more dominant because of the exceeding effects of buoyancy force rather than gravity force. Normally, the addition of hybrid nanoparticles enhances the thermal conduction heat transfer with with the less effect of natural convection inside the heat sink. Indeed, this is due to the fact that, without insertion of the nanoparticles, the small part of solid PCM remaining plays the role of a heat sink which decreases the temperature due to the temperature gradient between the heat generating source and the ambient.

3.2. Evaluation of liquid–fraction contours

The contours representing the evolution of the HNCPCM melting front are shown in the Figure 6 for a HNCPCM based heat sink at $\chi = 0:0$ and $\chi = 1:3$ of Ag:GO hybrid nanoparticles. To clearly show the evolution of the melting front in both cases, the melting process is represented at different times.

The solid and liquid regions of the HNCPCM are shown in blue and red, respectively. At 300 s, it is clear that the melting process begins directly above the heat source and along the left and right side walls of the heat sink due to the thermal inertia of the heat sink. This

17

Static Temperature

[k] 296.00 297.95 299.90 301.85 303.80 305.75 307.70 309.65 311.60 313.55 315.50 317.45 319.40 322.00

(a) 300 s, $\chi = 0{:}0$ (b) 300 s, $\chi = 1{:}3$

(c) 600 s, $\chi = 0{:}0$ (d) 600 s, $\chi = 1{:}3$

(e) 900 s, $\chi = 0{:}0$ (f) 900 s, $\chi = 1{:}3$

(g) 1200 s, $\chi = 0{:}0$ (h) 1200 s, $\chi = 1{:}3$

(i) 1500 s, $\chi = 0{:}0$ (j) 1500 s, $\chi = 1{:}3$
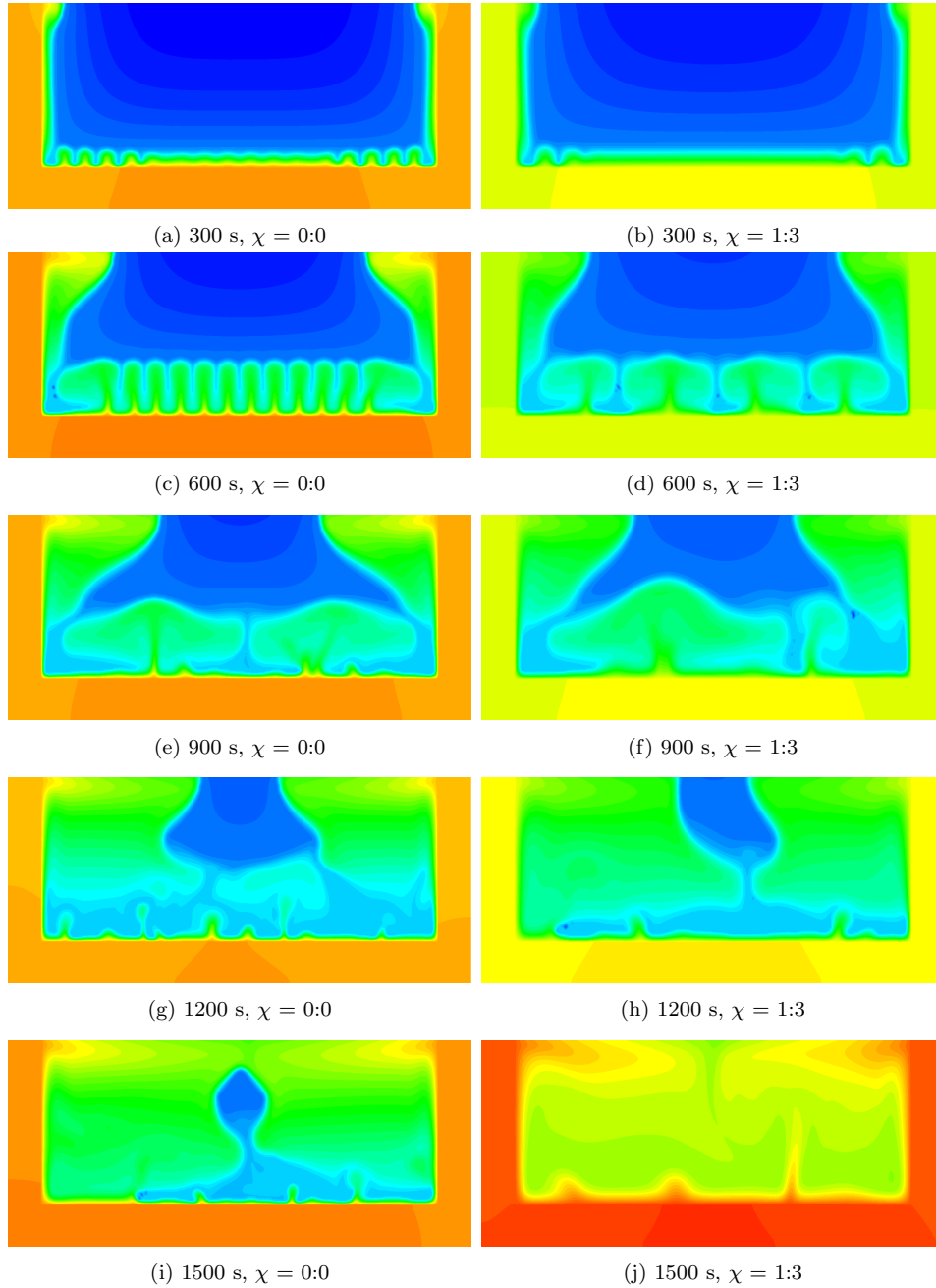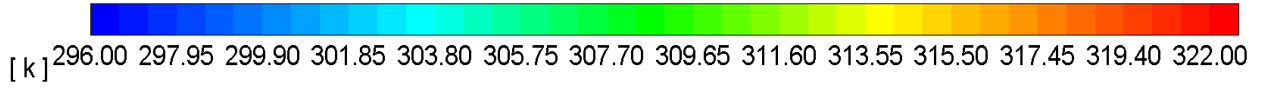
Figure 5: *Variation of isotherms contours at various t and χ for HNCPCM filled heat sink.*

gives rise to a circulation of liquid PCM under the effect of the buoyancy force exerted by gravity. This evolution of the melting front is explained by the fact that the heat transfer is purely conductive, at this stage, between the heat sink walls and the PCM layers in contact. At 600 s and 900 s, the melting front is clearly advancing in the region above the electronic

18

component and at the top of both the right and left sides of the heat sink. In addition, the melting front advances rapidly in the case of HNCPCM with insertion of the hybrid nanoparticles compared to the case of PCM alone. This is directly related to the increase of the heat transfer rate by improving the effective thermal conductivity. As the amount of liquid PCM increases, the hot liquid PCM rises towards the melting front and the cold liquid PCM falls towards the bottom. When the hot liquid PCM comes into contact with the melting front, it releases heat to the melting front while causing the mass of the adjacent solid PCM to melt and subsequently cause the melting front to move. This flow structure clearly justifies the major contribution of natural convection for the passive cooling of the electronic component.

At 1200 s, the melting front advances and the value of the liquid fraction increases. It is clear that the highest rate of the liquid fraction is recorded in the case of HCNPCM. The majority of the heat sink domain contains a liquid phase while the amount of the remaining solid phase is small. This is due to the effects of buoyancy combined with natural convection.

At 1500 s, the complete melting of the HNCPCM is observed in the case of a hybrid nanoparticles insertion. In the case of a pure PCM, there is still a quantity of solid PCM located approximately in the centre of the enclosure. An evolution of the melting front in the upper part of the enclosure is clear and is mainly due to the existence of the heat sink having a thermal inertia capable of transferring heat from the electronic component to the right and left sides. This justifies the existence of a certain amount of solid PCM in centre of the enclosure. The insertion of hybrid nanoparticles improves the rate of heat transfer by conduction or convection within the PCM and subsequently an acceleration of the melting process will take place. It is important to mention that the amount of solid PCM remaining in the case of a pure PCM contributes to the decrease of the operating temperature of the electronic component because it reacts as a heat sink absorbing generated heat and which can cause their melting.

3.3. Effect of hybrid nanoparticles volume fraction ratios

3.3.1. Evaluation of average temperature, effective thermal conductivity and thermal effusivity

The distribution of average temperature of heat sink (T_{HS}), effective thermal conductivity (k_{eff}), and effective thermal effusivity (e_{eff}) for different ratios and combinations of hybrid nanoparticles are presented in Figures 7a, 7b and 7c, respectively, at a constant input
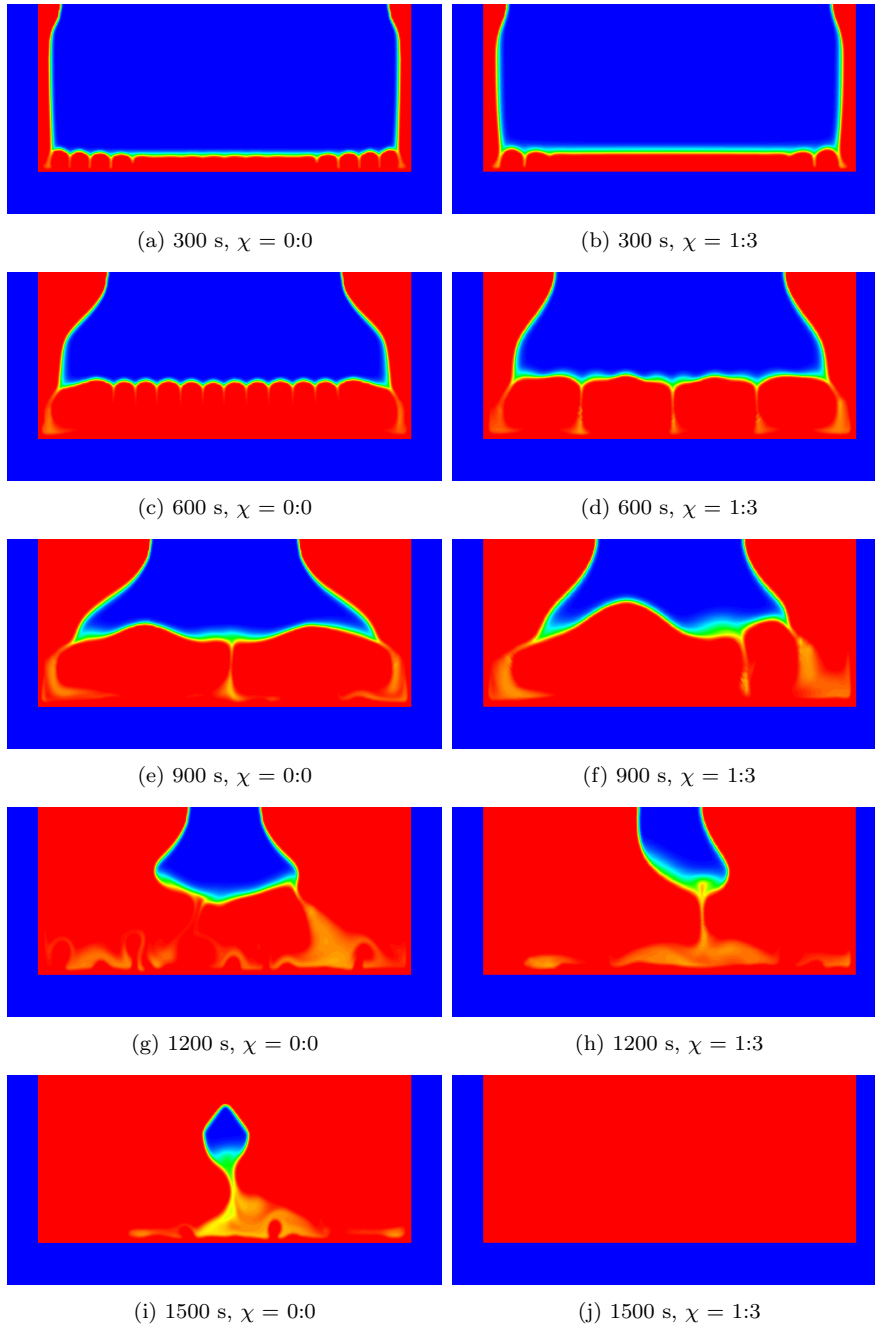
Figure 6: *Variation of f_l at various t and χ of HNCPCM filled heat sink.*

power level.

For the evolution of the average temperature of the heat sink, it is clear that for all combinations of inserted nanoparticles, the average temperature pattern is divided into three main steps. A first step where the temperature starts to increase rapidly and linearly in a similar way in all cases of inserted nanoparticles. A difference is clearly visible in the case of

a pure PCM without nanoparticles insertion. This behaviour clearly proves that this step is governed by a purely conductive heat transfer mode. This heat transfer mode is intensified in the presence of inserted nanoparticles. A second stage will take place. Between the end of the first stage and the beginning of the second, there is a slight decrease in temperature, reflecting a competition between cooling and heating of the electronic component. In fact, it is a competition between conduction and natural convection for heating and cooling of the electronic component. This situation does not last long and it will be finalized by a triumph of natural convection which will guarantee a practically constant evolution of the temperature. In fact, it is a period of latent heat storage at constant temperature and is described by a phase change plateau. The third and final stage is characterized by a further increase in temperature. The latter begins to rise, again, in a rapid manner. In this stage thermal conduction and natural convection coexist at the same time.

As for the effect of the insertion of GO and Ag nanoparticles within the basic PCM, it is clear that they clearly contribute to the decrease of the average temperature. This is mainly due to the improvement of heat transfer. Moreover, among the compositions of the inserted nanoparticles, mono or hybrid, considered in this study, the insertion of hybrid nanoparticles of composition 2% for each type of nanoparticles decreased the heat sink temperature in a very significant way compared to the other compositions. Moreover, this composition is the one that guarantees a long latent storage period where the temperature remains practically constant. It should be noted that during this period the electronic component operates far from any risk of failure. This is an important result giving major importance to the insertion of hybrid nanoparticles instead of mono nanoparticles.

To further prove this behaviour found by hybrid nanoparticles insertion, the effect of insertion of mono and hybrid nanoparticles on the evolution of k_{eff} and e_{eff} was evaluated and the results are presented in Figures 7b and 7c, respectively. A quick analysis of the results prove that the insertion of hybrid nanoparticles into the base PCM not only improves the k_{eff} but also the e_{eff}. The latter parameter plays an indispensable role in the exchange of thermal energy with the external environment. A higher rate of improvement in k_{eff} and e_{eff} is recorded for the hybrid composition with insertion of two equal volumetric fractions of nanoparticles. This composition improves heat transfer within the cooling model. Hence the importance of insertion of hybrid nanoparticles instead of mono nanoparticles.

21
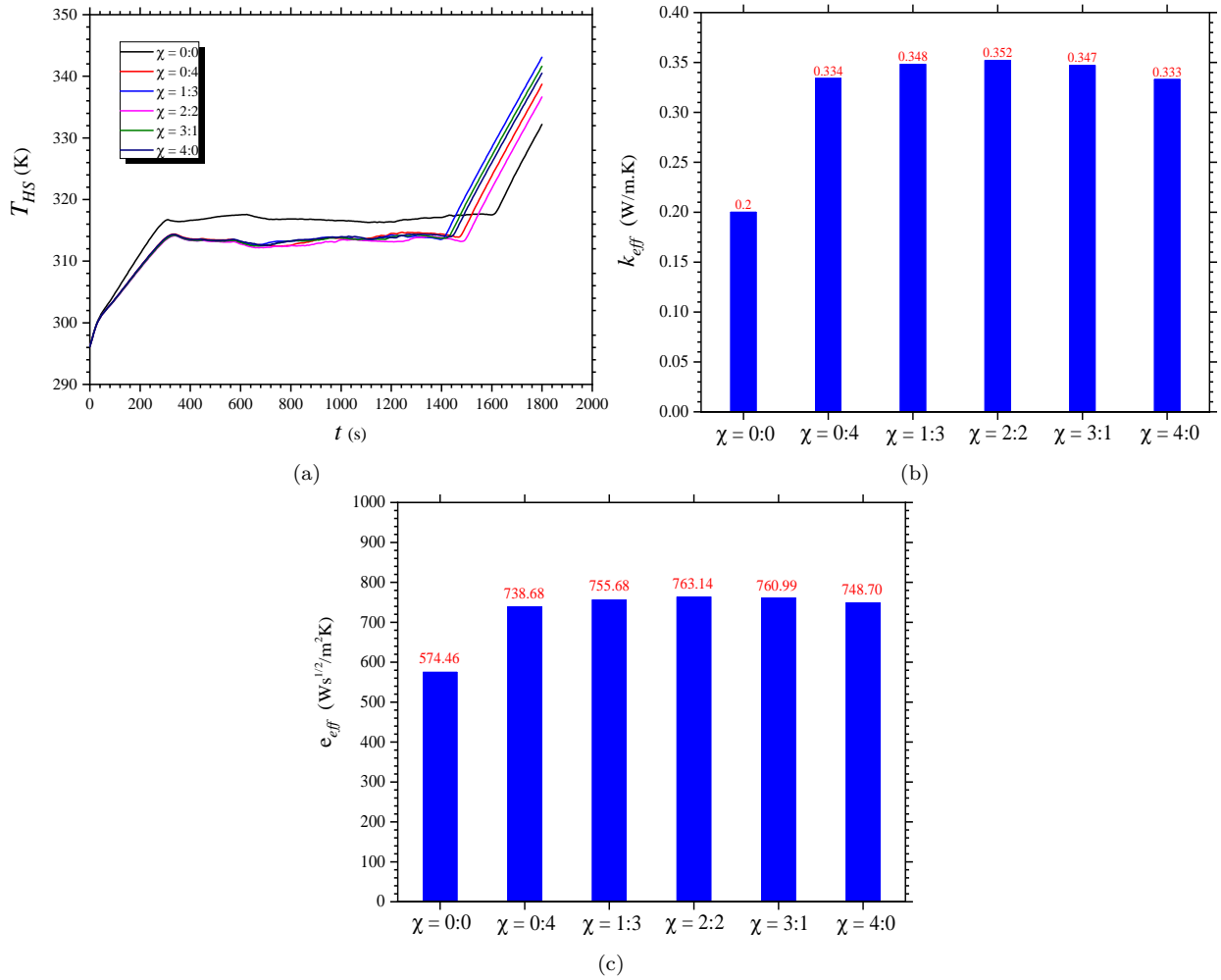
Figure 7: *Comparison of (a) T_{HS}, (b) k_{eff} and (c) e_{eff} for various χ of Ag-GO.*

3.3.2. Evaluation of liquid–fraction and melting time

The evolution of f_l and t_{melt} for different ratios of φ of Ag-GO is shown in Figures 8a and 8b, respectively, at a constant power level. It is clear that, by insertion of the nanoparticles, the melting process is accelerated. The maximum acceleration rate is obtained by insertion of the hybrid nanoparticles. The reduction of melting time is obtained of -8.83%, -12.93%, -7.57%, -11.67% and -10.73% with Ag:GO ratios of 0:4, 1:3, 2:2, 3:1, and 4:0, respectively. More precisely, this rate is obtained by inserting 0.0% of Ag and 3.0% of GO. With this composition, the melting time has decreased by 12.93%. With insertion of mono nanoparticles, the maximum decrease in melting time is obtained by inserting a fraction of 4.0% of Ag and that is equal to 10.73%. Hence, the reduction of the total melting time and the acceleration of the melting process is obtained by insertion of hybrid nanoparticles.

22
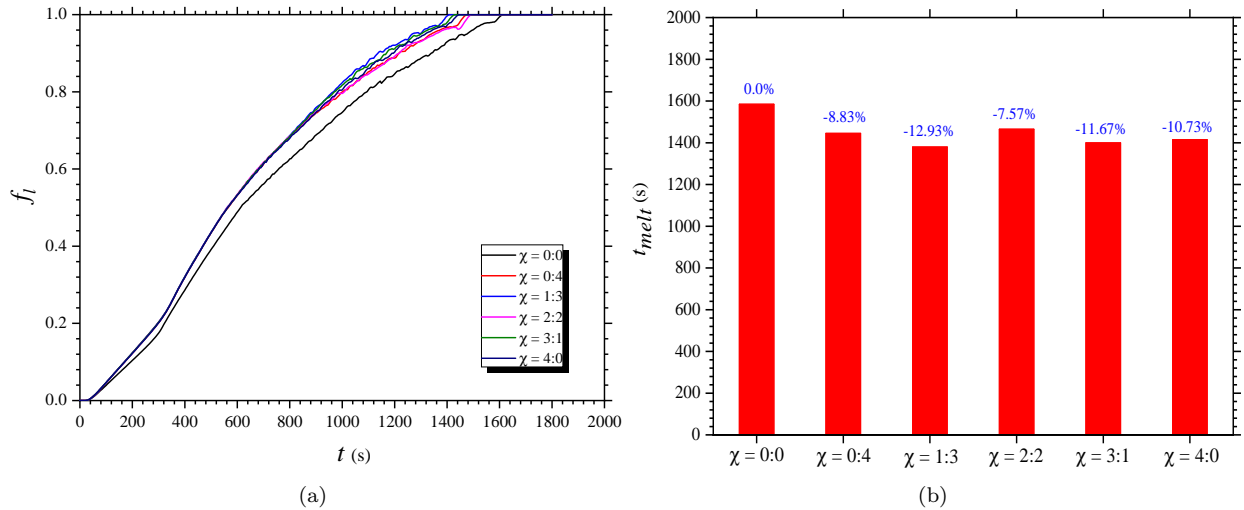
Figure 8: *Comparison of (a) f_l and (b) t_{melt} for various χ of Ag-GO.*

3.3.3. Evaluation of critical time and average transient temperature of heat sink.

The thermal performance of all cases of PCM and hybrid nanoparticles based heat sinks in terms of critical time and mean transient temperature is presented in Figure 9. The critical time for the heat sink to reach set point temperatures (SPTs) of 35 °C, 40 °C, and 45 °C is presented in Figure 9a for each combination of inserted hybrid nanoparticles. The results obtained group the time it takes heat sinks of different compositions of inserted nanoparticles to reach the indicated SPTs. These results can be clearly shown that the effect of the different combinations to reach the SPTs of 35 °C and 40 °C is almost negligible. This effect becomes important for the SPT of 45 °C. Indeed, the first two SPTs are reached at the first stage of temperature evolution which is not very sensitive to the effect of the combination of the inserted nanoparticles since thermal conduction reigns. The SPT of 45 °C is reached in the second stage where the contribution of natural convection exists and is sensitive to the combination of the inserted nanoparticles. Figure 9b shows the temperature reached in each case studied during an operating time of 900 s and 1800 s. A very important remark that is clear from the results found reveals that a very high temperature is reached during the first 900 s while the second 900 s gave rise only to a small temperature difference that does not exceed 30 K at most. This is due to the important effects of natural convection for the cooling of the electronic component during the second and third stage of temperature evolution. This second stage called the latent heat phase is the key region for passive cooling of electronic devices using PCM and nanoparticles based heat sinks.

23
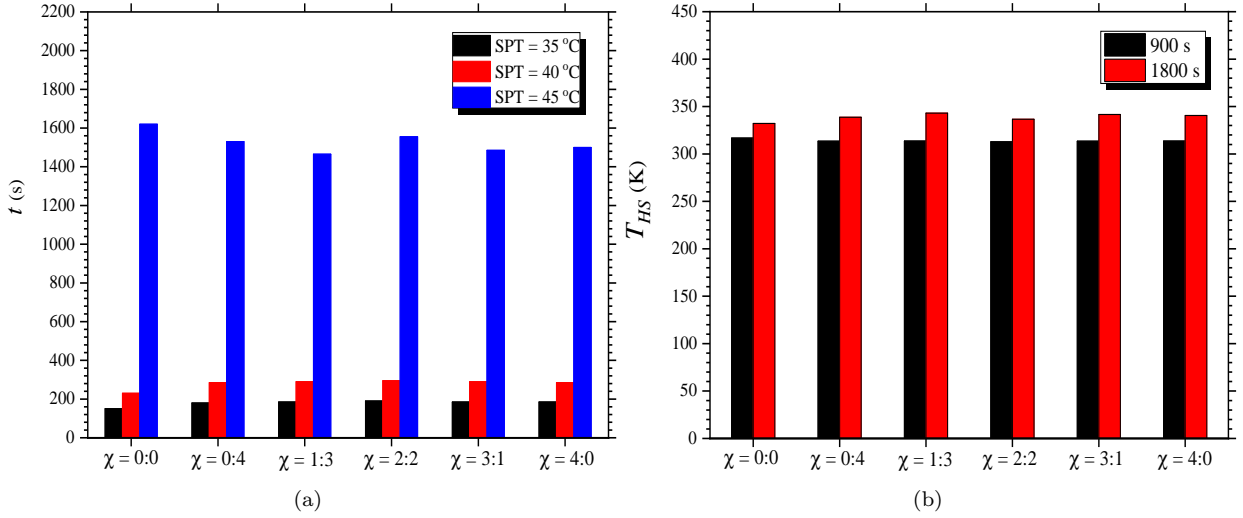
Figure 9: *Comparison of (a) critical time and (b) average transient temperature of heat sink for various χ of Ag-GO.*

3.3.4. Evaluation of Q, q, $\dot{Q}$ and $\dot{q}$ for various χ of Ag-GO hybrid nanoparticles.

An evaluation of thermal performance of Ag-GO hybrid nanoparticles dispersed HNCPCM base heat sink is presented in terms of heat storage capacity (Q), heat storage density (q), rate of heat transfer ($\dot{Q}$) and rate of heat transfer density ($\dot{q}$) for various χ of Ag-GO hybrid nanoparticles. The results are presented in Fig. 10 and summarized in Table 3 for three different phases of heating: pre-sensible, latent, and post-sensible. The heat storage and heat transfer analysis presents the amount of heat absorbed and transfer by the HNCPCM heat sink generated by an electronic component during operation. From Figs. 10a and 10c, it can be seen that a non-uniform trend in obtained for Q and $\dot{Q}$ which is due the effect of thermophysical properties of Ag and GO, and amount of mass of HNCPCM at different χ. Despite of that, q and $\dot{q}$ show a decreasing trend with the increase of Ag content or with the decrease of GO content for different χ because of the increase of mass from $\chi = 0:0$ to $\chi = 4:0$. Indeed, an insertion of nanoparticles within the base PCM increases the mass of the heat sink and significantly influences the effective thermophysical properties. The total mass of the HCNPCM is increase with the increase of ratio of φ. The increase in total mass of PCM is obtained of 4.73%, 15.24%, 25.77%, 36.33% and 46.91% with Ag:GO ratios of 0:4, 1:3, 2:2, 3:1 and 4:0, respectively, compare with 0:0 ratio of φ. A very less significant effect of Q and q is obtained while pre-sensible heating phase, however a remarkable effect of Q and q while latent heating phase which shows that HNCPCMs based heat sinks are very much effective for passive cooling of applications. The sight variation in ρ_{hncpcm} and c_{hncpcm} affects the Q, $\dot{Q}$, q and $\dot{q}$. The enhancement in $\dot{Q}$ is obtained of 3.81%, 8.65%, 2.35%,

24

7.41% and 6.25% with Ag:GO ratios of 0:4, 1:3, 2:2, 3:1 and 4:0, respectively. A gradual decreasing trend in q and $\dot{q}$ can be seen from Figs. 10b and 10d, respectively. The reduction in q is obtained of -9.63%, -17.91%, -24.78%, -30.41% and -35.43% with Ag:GO ratios of 0:4, 1:3, 2:2, 3:1 and 4:0, respectively, compared to the 0:0 of Ag-GO hybrid nanoparticles. Similarly, the reduction in $\dot{q}$ is obtained of -0.87%, -5.72%, -18.62%, -21.21% and -27.68% with Ag:GO ratios of 0:4, 1:3, 2:2, 3:1 and 4:0, respectively, compared to the 0:0 of Ag-GO hybrid nanoparticles. The results show that the insertion of Ag:GO hybrid nanoparticles with 1:3 volume fraction ratio guarantees a maximum $\dot{Q}$ and $\dot{q}$ compared to the insertion of mono nanoparticles and pure PCM. Therefore, the insertion of hybrid nanoparticles within a basic PCM is suggested for efficient thermal management of electronic components.
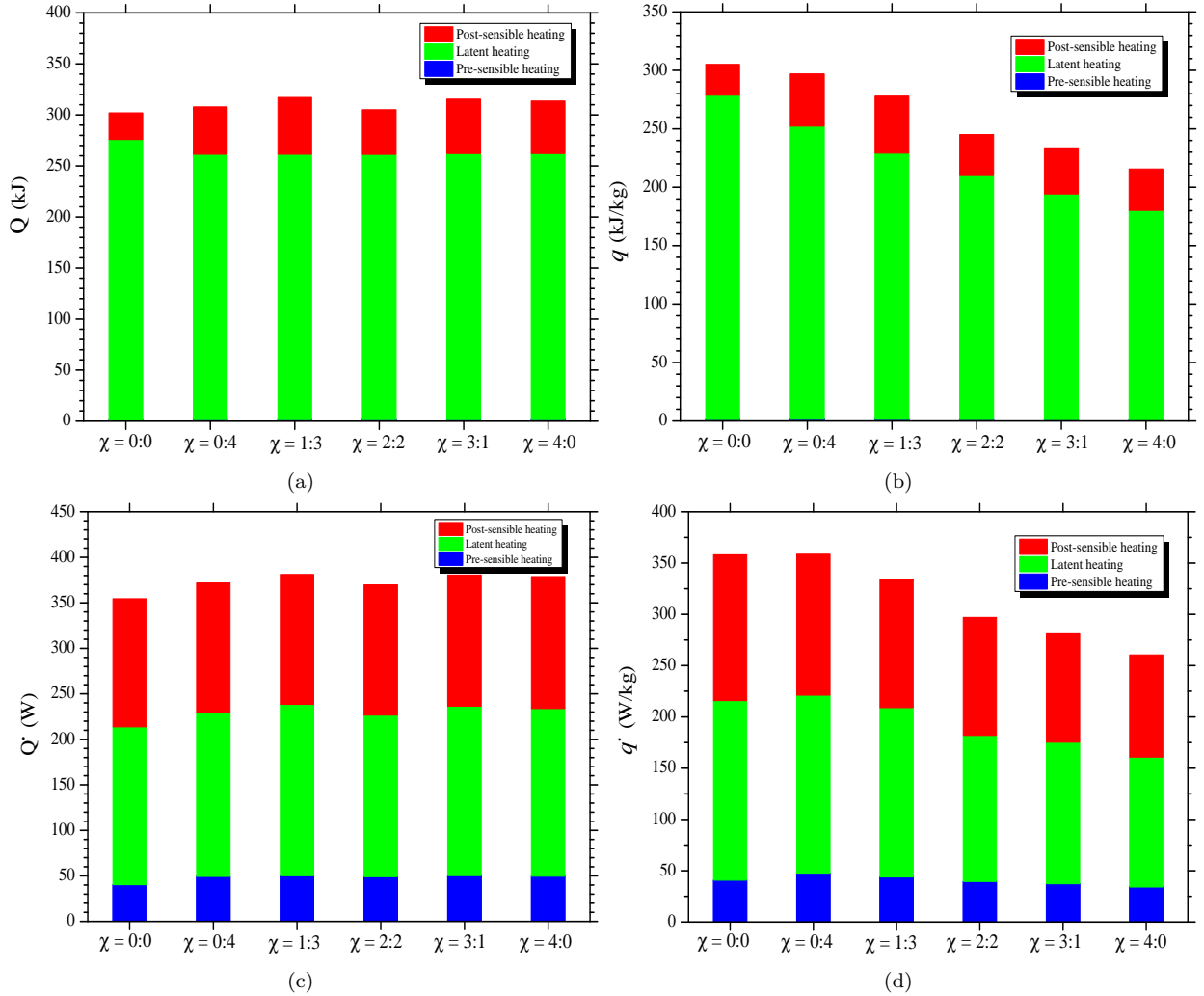
Figure 10: *Comparison of (a) Q, (b) q, (c) $\dot{Q}$ and (d) $\dot{q}$ of HNCPCM filled heat heat sink for various χ of GO-Ag hybrid nanoparticles.*

Table 3: The Q, q, $\dot{Q}$ and $\dot{q}$ of various χ of Ag-GO hybrid nanoparticles dispersed HNCPCM based heat sink.

	Pre-sensible heating	Latent heating	Post-sensible heating	Pre-sensible heating	Latent heating	Post-sensible heating
	Q (kJ)			q (kJ/kg)		
$\chi = 0{:}0$	1.21	274.79	26.04	1.22	277.56	26.31
$\chi = 0{:}4$	1.48	260.07	46.33	1.43	250.84	44.69
$\chi = 1{:}3$	1.50	259.94	55.66	1.32	227.84	48.78
$\chi = 2{:}2$	1.47	259.95	43.67	1.18	208.77	35.07
$\chi = 3{:}1$	1.51	260.70	53.27	1.12	193.16	39.47
$\chi = 4{:}0$	1.49	260.64	51.46	1.02	179.21	35.38
	$\dot{Q}$ (W)			$\dot{q}$ (W/kg)		
$\chi = 0{:}0$	40.37	173.37	140.77	40.77	175.12	142.19
$\chi = 0{:}4$	49.36	179.98	142.56	47.60	173.59	137.50
$\chi = 1{:}3$	50.15	188.36	142.71	43.96	165.10	125.09
$\chi = 2{:}2$	49.17	177.44	143.17	39.49	142.51	114.98
$\chi = 3{:}1$	50.31	186.21	143.98	37.28	137.97	106.68
$\chi = 4{:}0$	49.67	184.20	144.97	34.15	126.65	99.68

3.4. Effect of hybrid nanoparticles shape factor

The effect of the shape of the inserted nanoparticles is evaluated. Four shapes of nanoparticles are inserted to reveal their effect on the thermal response of the heat sink for cooling the electronic component. The results are presented with $\chi = 1{:}3$ ratio of Ag:GO hybrid nanoparticles dispersed HNCPCM based heat sink.

3.4.1. Evaluation of average temperature, effective thermal conductivity and thermal effusivity

The dependence of the mean heat sink temperature (T_{HS}), effective thermal conductivity (k_{eff}), and effective thermal effusivity (e_{eff}) on the shape of the nanoparticles is shown in Figure 11. The evolution of the T_{HS} always keeps the three-step variation pattern. These steps are described in detail in the previous section. Always, the evolution starts with a stage where it varies linearly and rapidly and where conduction is the prevailing heat transfer. The second stage is characterized by the strong existence of natural convection and especially its contribution to the cooling of the electronic component. The last stage is characterized by a further increase in temperature and in which the existence of conduction and natural convection is mutual. As for the effect of the insertion of nanoparticles of different shapes, it is clear that the more the shape factor increases, the more the operating temperature decreases. This decrease is clear for nanoparticles with $sf = 16.1$. This effect is most noticeable in the second stage of average temperature evolution where the contribution of natural convection is important. In the first and second stages, this effect is almost negligible and the conductive regime is considered stable. Similarly, by increasing the sf of the nanoparticles, the duration of the latent phase decreases, knowing that this duration characterizes the period when the electronic component decreases far from any failure. A

26

choice between low-temperature operation and reduced latent phase duration or the reverse is imposed. To prove this behaviour, the k_{eff} and the e_{eff} and their dependence on the sf of the nanoparticles were evaluated. It can be seen that by inserting nanoparticles with a $sf = 16.1$, an improvement of 66.38% and 81.54% is obtained for k_{eff} and e_{eff}, respectively. This is a very significant rate of improvement and gives a high importance to the insertion of nanoparticles with a high shape-factor value.
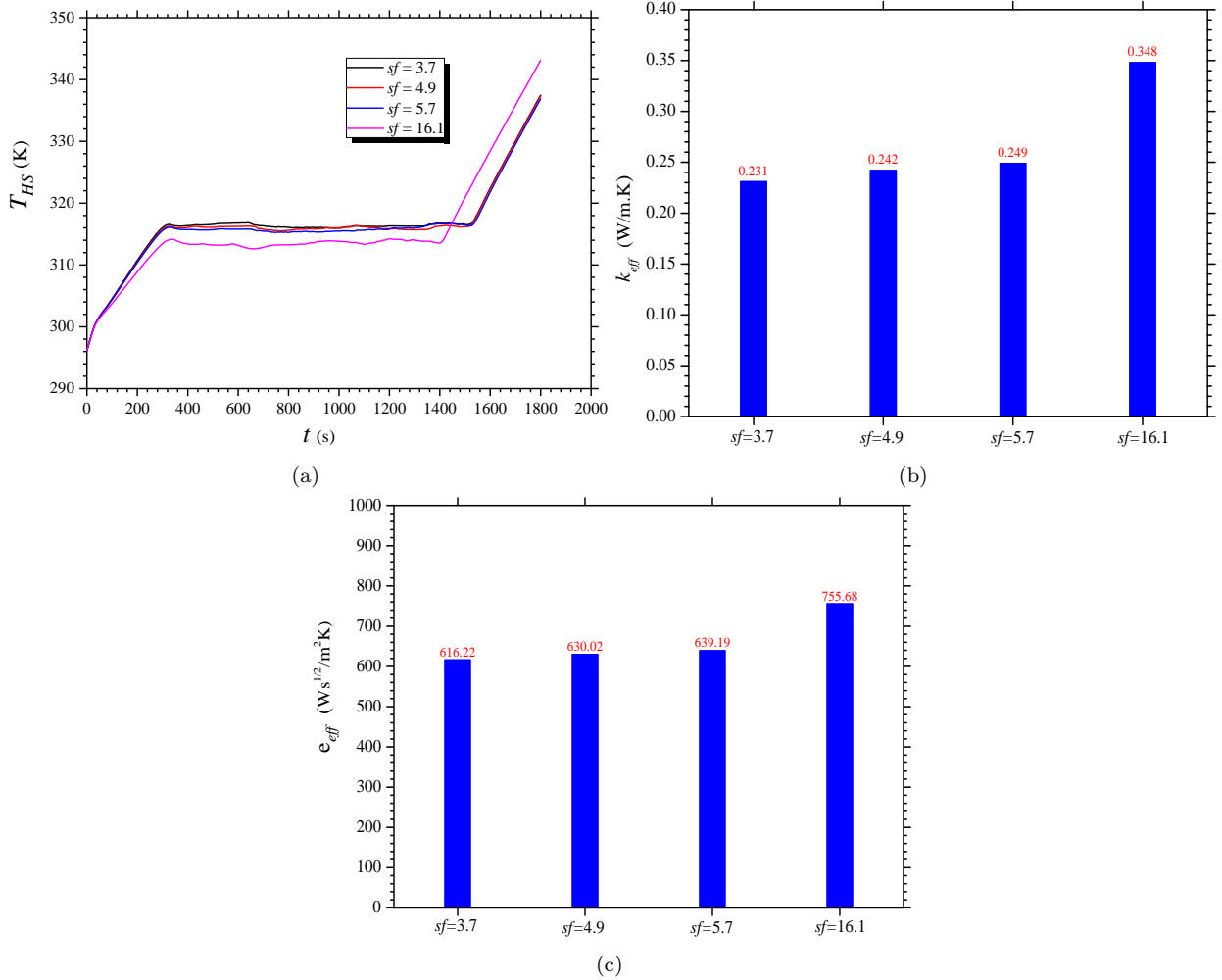
Figure 11: *Comparison of (a) T_{HS}, (b) k_{eff} and (c) e_{eff} for various sf of HNCPCM filled heat sink.*

3.4.2. Evaluation of liquid–fraction and melting time

The Figure 12 shows the results obtained for the variation in the f_l of the molten PCM and the required . These results are presented as a function of the sf of the inserted nanoparticles with constant power level. It can be seen that the higher the sf increases, the higher the liquid fraction and subsequently the shorter the t_{melt}. The insertion of nanoparticles with a high sf clearly accelerates the melting process due to the significant improvement of

the k_{eff} and e_{eff}. The t_{melt} has been reduced by 120 s by inserting nanoparticles with a sf of 16.1 with a percentage reduction of 8%.
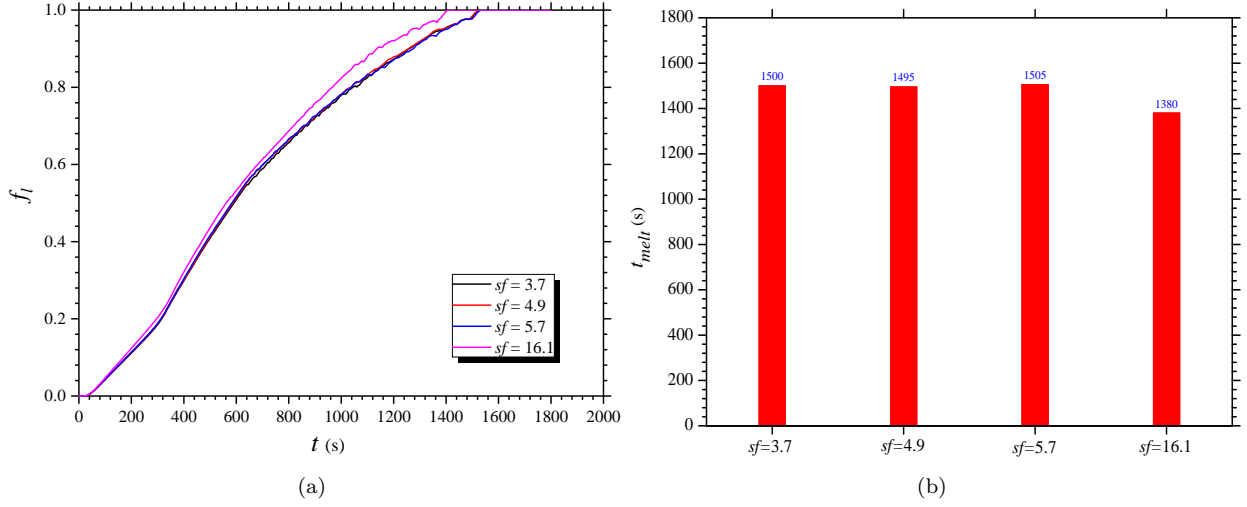
Figure 12: *Comparison of (a) f_l and (b) t_{melt} for various sf of HNCPCM filled heat sink.*

3.4.3. Evaluation of critical time and average transient temperature of heat sink

The effect of the shape factor of nanoparticles on the critical time to reach the indicated SPTs and the average transient temperature recorded for two different durations is shown in Figure 13. It is clear that increasing the sf from 3.7 to 16.1 decreases the time required to reach the SPT of 45 °C and increases the time to reach the SPT of 40 °C. In addition, the effect of the variation in the shape factor of nanoparticles has a limited effect on the temperature recorded during 900 s and 1800 s. A slight difference appears in the case of insertion of nanoparticles with a sf of 16.1 where the temperature recorded during 1800 s of operation of the electronic component. In fact, the increase in the sf of nanoparticles improves the thermal conduction very little while causing a temperature increase in the third stage of melting where the existence of natural convection and conduction is mutual.

3.4.4. Evaluation of Q, q, $\dot{Q}$ and $\dot{q}$ for various sf of Ag-GO hybrid nanoparticles.

The thermal performance analysis is evaluated by varying the different sf values of Ag-GO hybrid nanoparticles in terms of heat storage capacity (Q), heat storage density (q), rate of heat transfer ($\dot{Q}$) and rate of heat transfer density ($\dot{q}$). The results of Q, q, $\dot{Q}$ and $\dot{q}$ are presented in Fig. 14 and summarized in Table 4. The slight variations in Q, q, $\dot{Q}$ and $\dot{q}$ are observed for sf of 3.7, and 4.9. However, lower Q and q values, and higher $\dot{Q}$ and $\dot{q}$ are observed at $sf = 16.1$ because of the higher thermal conductivity of HNCPCM at 16.1 sf value of Ag-GO hybrid nanoparticles. The maximum value of $\dot{Q}$ and

28
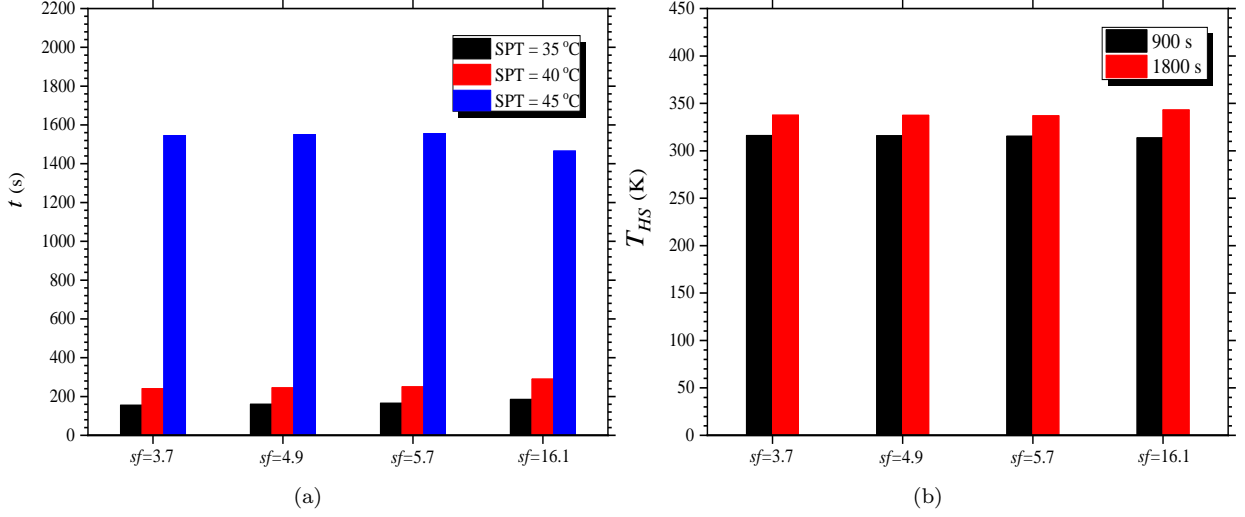
Figure 13: *Comparison of (a) critical time and (b) average transient temperature of heat sink for various sf of HNCPCM filled heat sink.*

Table 4: The Q, q, $\dot{Q}$ and $\dot{q}$ of various sf of Ag-GO hybrid nanoparticles dispersed HNCPCM based heat sink.

	Pre-sensible heating	Latent heating	Post-sensible heating	Pre-sensible heating	Latent heating	Post-sensible heating
	Q (kJ)			q (kJ/kg)		
sf=3.7	1.28	263.37	38.32	1.12	230.86	33.59
sf=4.9	1.31	262.59	39.21	1.15	230.17	34.37
sf=5.7	1.32	263.54	37.65	1.16	231.00	33.00
sf=16.1	1.50	259.94	55.66	1.32	227.84	48.78
	$\dot{Q}$ (W)			$\dot{q}$ (W/kg)		
sf=3.7	42.74	175.58	141.94	37.46	153.90	124.42
sf=4.9	43.56	175.64	142.57	38.18	153.96	124.96
sf=5.7	44.10	175.11	142.07	38.66	153.49	124.53
sf=16.1	50.15	188.36	142.71	43.96	165.10	125.09

$\dot{q}$ are obtained of 188.36 W and 165.10 W/kg, respectively. However, the minimum values of 259.94 kJ and 227.84 kJ/kg are obtained for Q and q by inserting hybrid nanoparticles of Ag-GO with a sf of 16.1. Thus, it can be revealed that by inserting high sf of Ag-GO hybrid nanoparticles, the thermal performance within the HNCPCM is clearly improved and subsequently the extraction of the heat generated by the electronic component becomes easy result in provided the effective cooling of the electronic component. Practical applications for the cooling of electronic components require consideration of these factors, which clearly influence the passive cooling process of the electronic component.

4. Conclusions

A numerical investigation was carried out to explore the effect of hybrid nanoparticles added nanocomposite phase change material (HNCPCM) filled heat sink for passive cooling enhancement of portable electronic devices. Six different ratios of constant volume fraction and four different shape factor values are varied of Ag-GO hybrid nanoparticles. The

29
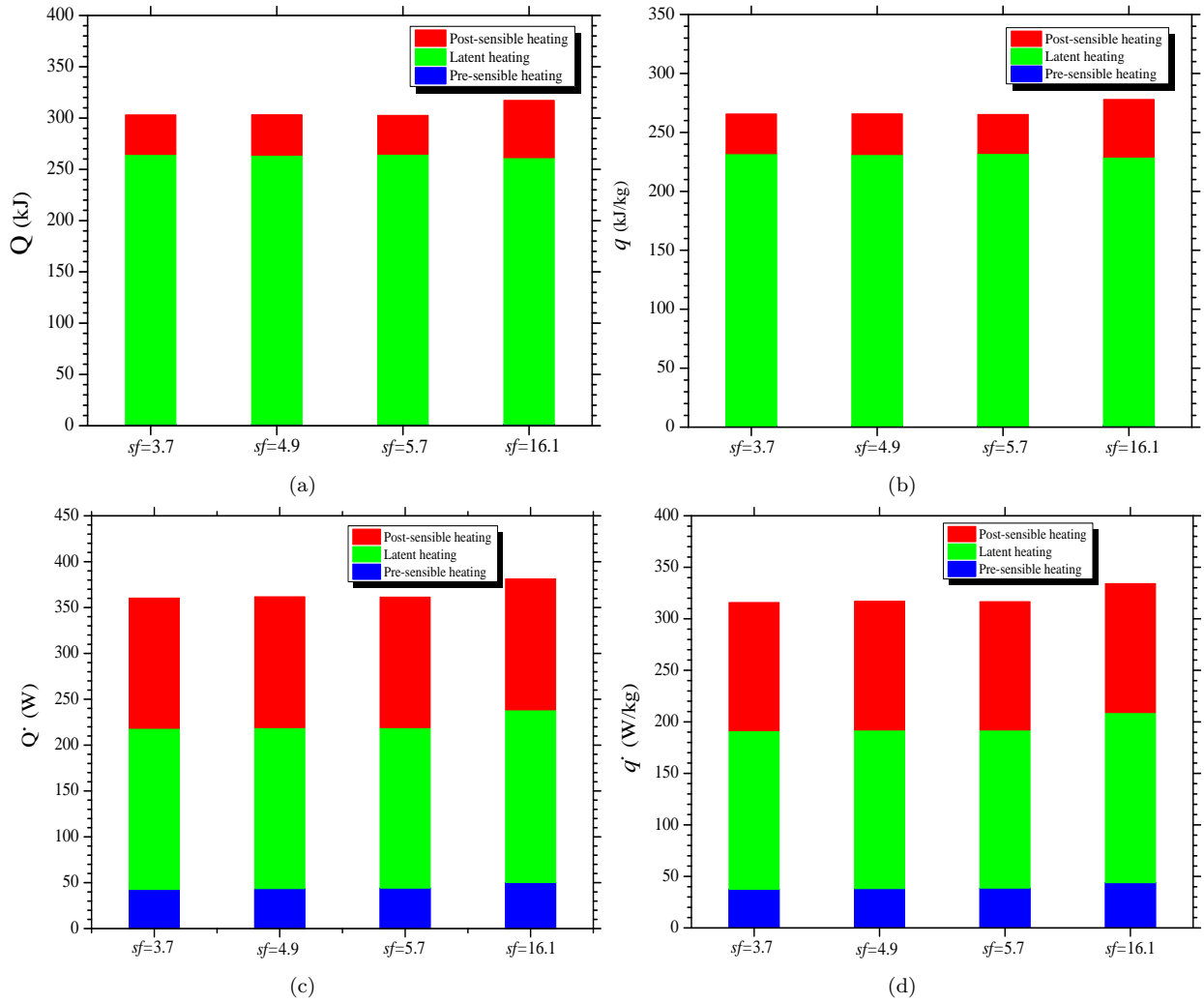
Figure 14: *Comparison of (a) Q, (b) q, (c) $\dot{Q}$ and (d) $\dot{q}$ of HNCPCM filled heat heat sink for various sf of GO-Ag hybrid nanoparticles.*

isotherm and liquid-fraction contours are presented to visualize the solid-liquid interface and isotherm distribution. Thermal process enhancement is studied by comparing the melting time, heat storage capacity, heat storage density, rate of heat transfer, and rate of heat transfer density. The following are the main outcomes and suggestion are highlighted from the results:

- By adding the Ag-GO hybrid nanoparticles improved the melting process of PCM inside the heat sink. The heat conduction flow was observed at initially. Further heat convection flow is observed during phase transformation because of buoyancy and gravitational effects. Lastly, again heat conduction flow is observed after complete melting of HNCPCM.

- The higher thermal conductivity and thermal effusivity are obtained by adding he hybrid nanoparticles compared to the pure RT-28HC. The enhancement in thermal

30

conductivity and thermal effusivity are obtained of 73.85% and 31.55%, respectively, with 1:3 ratio of Ag:GO added HNCPCM heat sink. The optimum ratio of 1:3 is revealed of Ag:GO showing the highest rate of heat transfer with 8.65% enhancement compared without adding nanoparticles.

- The lower heat sink temperature is obtained with HNCPCM filled heat sink compared to pure RT-28HC filled heat sink. With the increase of volume fraction ratio of Ag:GO, latent heating phase reduces and the maximum reduction of melting time is obtained of 12.93%, with Ag:GO ratio of 1:3.

- The shape factor of 16.1 shows the lowest heat sink temperature, higher thermal conductivity and thermal effusivity, highest heat transfer rate of 188.36 W and rate of heat transfer density of 165.10 W/kg.

To sum up the current study, it is suggested that using 1:3 ratio of Ag:GO hybrid nanoparticles and 16.1 shape factor nanocomposite phase change material based heat sink proved the efficient and effective passive thermal cooling performance of portable electronic devices.

Conflict of interest

The authors declare no conflict of interest regarding this research article.

References

[1] W. R. Humphries, E. I. Griggs, A design handbook for phase change thermal control and energy storage devices, NASA Huntsville, AL, 1977.

[2] S. S. Murshed, Advanced Cooling Technologies and Applications, BoD–Books on Demand, 2019.

[3] L. T. Yeh, Review of heat transfer technologies in electronic equipment, Journal of Electronic Packaging 117 (4) (1995) 333–339. `doi:10.1115/1.2792113`.

[4] M. Goodarzi, I. Tlili, Z. Tian, M. R. Safaei, Efficiency assessment of using graphene nanoplatelets-silver/water nanofluids in microchannel heat sinks with different cross-sections for electronics cooling, International Journal of Numerical Methods for Heat & Fluid Flow 30 (1) (2019) 347–372. `doi:10.1108/hff-12-2018-0730`.

[5] H. Arasteh, R. Mashayekhi, M. Goodarzi, S. H. Motaharpour, M. Dahari, D. Toghraie, Heat and fluid flow analysis of metal foam embedded in a double-layered sinusoidal heat sink under local thermal non-equilibrium condition using nanofluid, Journal of Thermal Analysis and Calorimetry 138 (2) (2019) 1461–1476. `doi:10.1007/s10973-019-08168-x`.

[6] M. Bahiraei, M. Jamshidmofid, M. Goodarzi, Efficacy of a hybrid nanofluid in a new microchannel heat sink equipped with both secondary channels and ribs, Journal of Molecular Liquids 273 (2019) 88–98. `doi:10.1016/j.molliq.2018.10.003`.

[7] A. A. A. Arani, O. A. Akbari, M. R. Safaei, A. Marzban, A. A. Alrashed, G. R. Ahmadi, T. K. Nguyen, Heat transfer improvement of water/single-wall carbon nanotubes (SWCNT) nanofluid in a novel design of a truncated double-layered microchannel heat sink, International Journal of Heat and Mass Transfer 113 (2017) 780–795. `doi:10.1016/j.ijheatmasstransfer.2017.05.089`.

[8] M. Bahiraei, S. Heshmatian, M. Goodarzi, H. Moayedi, CFD analysis of employing a novel ecofriendly nanofluid in a miniature pin fin heat sink for cooling of electronic components: Effect of different configurations, Advanced Powder Technology 30 (11) (2019) 2503–2516. `doi:10.1016/j.apt.2019.07.029`.

[9] S. K. Sahoo, M. K. Das, P. Rath, Application of TCE-PCM based heat sinks for cooling of electronic components: A review, Renewable and Sustainable Energy Reviews 59 (2016) 550–582. doi:10.1016/j.rser.2015.12.238.

[10] S. S. Haghighi, H. Goshayeshi, M. R. Safaei, Natural convection heat transfer enhancement in new designs of plate-fin based heat sinks, International Journal of Heat and Mass Transfer 125 (2018) 640–647. doi:10.1016/j.ijheatmasstransfer.2018.04.122.

[11] W. Liu, O. Malekahmadi, S. A. Bagherzadeh, M. Ghashang, A. Karimipour, S. Hasani, I. Tlili, M. Goodarzi, A novel comprehensive experimental study concerned graphene oxide nanoparticles dispersed in water: Synthesise, characterisation, thermal conductivity measurement and present a new approach of RLSF neural network, International Communications in Heat and Mass Transfer 109 (2019) 104333. doi:10.1016/j.icheatmasstransfer.2019.104333.

[12] M. Goodarzi, I. Tlili, H. Moria, T. A. Alkanhal, R. Ellahi, A. E. Anqi, M. R. Safaei, Boiling heat transfer characteristics of graphene oxide nanoplatelets nano-suspensions of water-perfluorohexane (c6f14) and water-n-pentane, Alexandria Engineering Journal 59 (6) (2020) 4511–4521. doi:10.1016/j.aej.2020.08.003.

[13] A. Arshad, M. Jabbal, Y. Yan, J. Darkwa, The micro-/nano-PCMs for thermal energy storage systems: A state of art review, International Journal of Energy Research 43 (11) (2019) 5572–5620. doi:10.1002/er.4550.

[14] C. S. Miers, A. Marconnet, Experimental investigation of composite phase change material heat sinks for enhanced passive thermal management, Journal of Heat Transfer 143 (1) (2020) 013001. doi:10.1115/1.4048620.

[15] H. M. Ali, A. Arshad, Experimental investigation of n-eicosane based circular pin-fin heat sinks for passive cooling of electronic devices, International Journal of Heat and Mass Transfer 112 (2017) 649–661. doi:10.1016/j.ijheatmasstransfer.2017.05.004.

[16] H. M. Ali, A. Arshad, M. Jabbal, P. Verdin, Thermal management of electronics devices with PCMs filled pin-fin heat sinks: A comparison, International Journal of Heat and

Mass Transfer 117 (2018) 1199–1204. `doi:10.1016/j.ijheatmasstransfer.2017.10.065`.

[17] H. M. Ali, A. Arshad, M. M. Janjua, W. Baig, U. Sajjad, Thermal performance of LHSU for electronics under steady and transient operations modes, International Journal of Heat and Mass Transfer 127 (2018) 1223–1232. `doi:10.1016/j.ijheatmasstransfer.2018.06.120`.

[18] H. M. Ali, M. J. Ashraf, A. Giovannelli, M. Irfan, T. B. Irshad, H. M. Hamid, F. Hassan, A. Arshad, Thermal management of electronics: An experimental analysis of triangular, rectangular and circular pin-fin heat sinks for various PCMs, International Journal of Heat and Mass Transfer 123 (2018) 272–284. `doi:10.1016/j.ijheatmasstransfer.2018.02.044`.

[19] A. Arshad, H. M. Ali, W.-M. Yan, A. K. Hussein, M. Ahmadlouydarab, An experimental study of enhanced heat sinks for thermal management using n-eicosane as phase change material, Applied Thermal Engineering 132 (2018) 52–66. `doi:10.1016/j.applthermaleng.2017.12.066`.

[20] A. Arshad, H. M. Ali, S. Khushnood, M. Jabbal, Experimental investigation of PCM based round pin-fin heat sinks for thermal management of electronics: Effect of pin-fin diameter, International Journal of Heat and Mass Transfer 117 (2018) 861–872. `doi:10.1016/j.ijheatmasstransfer.2017.10.008`.

[21] A. Arshad, H. M. Ali, M. Ali, S. Manzoor, Thermal performance of phase change material (PCM) based pin-finned heat sinks for electronics devices: Effect of pin thickness and PCM volume fraction, Applied Thermal Engineering 112 (2017) 143–155. `doi:10.1016/j.applthermaleng.2016.10.090`.

[22] Z. Qu, W. Li, W. Tao, Numerical model of the passive thermal management system for high-power lithium ion battery by using porous metal foam saturated with phase change material, International Journal of Hydrogen Energy 39 (8) (2014) 3904–3913. `doi:10.1016/j.ijhydene.2013.12.136`.

[23] Y. Li, L. Gong, M. Xu, Y. Joshi, A review of thermo-hydraulic performance of metal foam and its application as heat sinks for electronics cooling, Journal of Electronic Packaging`doi:10.1115/1.4048861`.

34

[24] R. Kothari, S. K. Sahu, S. I. Kundalwal, P. Mahalkar, Thermal performance of phase change material-based heat sink for passive cooling of electronic components: An experimental study, International Journal of Energy Research 45 (4) (2020) 5939–5963. `doi:10.1002/er.6215`.

[25] A. Arshad, M. Jabbal, Y. Yan, Thermal performance of PCM-based heat sink with partially filled copper oxide coated metal-foam for thermal management of microelectronics, in: 2020 19th IEEE Intersociety Conference on Thermal and Thermomechanical Phenomena in Electronic Systems (ITherm), IEEE, 2020. `doi:10.1109/itherm45881.2020.9190574`.

[26] N. S. Bondareva, B. Buonomo, O. Manca, M. A. Sheremet, Heat transfer inside cooling system based on phase change material with alumina nanoparticles, Applied Thermal Engineering 144 (2018) 972–981. `doi:10.1016/j.applthermaleng.2018.09.002`.

[27] N. S. Bondareva, B. Buonomo, O. Manca, M. A. Sheremet, Heat transfer performance of the finned nano-enhanced phase change material system under the inclination influence, International Journal of Heat and Mass Transfer 135 (2019) 1063–1072. `doi:10.1016/j.ijheatmasstransfer.2019.02.045`.

[28] A. V. Arasu, A. S. Mujumdar, Numerical study on melting of paraffin wax with al_2o_3 in a square enclosure, International Communications in Heat and Mass Transfer 39 (1) (2012) 8–16. `doi:10.1016/j.icheatmasstransfer.2011.09.013`.

[29] A. Arshad, M. Jabbal, L. Shi, J. Darkwa, N. J. Weston, Y. Yan, Development of TiO2/RT–35hc based nanocomposite phase change materials (NCPCMs) for thermal management applications, Sustainable Energy Technologies and Assessments (2020) 100865`doi:10.1016/j.seta.2020.100865`.

[30] R. Parameshwaran, K. Deepak, R. Saravanan, S. Kalaiselvam, Preparation, thermal and rheological properties of hybrid nanocomposite phase change material for thermal energy storage, Applied Energy 115 (2014) 320–330. `doi:10.1016/j.apenergy.2013.11.029`.

[31] Q. Ren, F. Meng, P. Guo, A comparative study of PCM melting process in a heat pipe-assisted LHTES unit enhanced with nanoparticles and metal foams by immersed boundary-lattice boltzmann method at pore-scale, International Journal of Heat and

Mass Transfer 121 (2018) 1214–1228. `doi:10.1016/j.ijheatmasstransfer.2018.01.046`.

[32] H. Wan, G. He, Z. Xue, W. Li, Numerical study and experimental verification on spray cooling with nanoencapsulated phase-change material slurry (NPCMS), International Communications in Heat and Mass Transfer 123 (2021) 105187. `doi:10.1016/j.icheatmasstransfer.2021.105187`.

[33] C. Liu, P. Du, B. Fang, Z. Li, B. Chen, Z. Rao, Experimental study on a functional microencapsulated phase change material for thermal management, International Communications in Heat and Mass Transfer 118 (2020) 104876. `doi:10.1016/j.icheatmasstransfer.2020.104876`.

[34] A. Tahmasebi, H. Zargartalebi, S. Mehryan, M. Ghalambaz, Thermal and hydrodynamic behavior of suspensions comprising nano-encapsulated phase change materials in a porous enclosure, International Communications in Heat and Mass Transfer 116 (2020) 104634. `doi:10.1016/j.icheatmasstransfer.2020.104634`.

[35] Y.-J. Chiu, W.-M. Yan, H.-C. Chiu, J.-H. Jang, G.-Y. Ling, Investigation on the thermophysical properties and transient heat transfer characteristics of composite phase change materials, International Communications in Heat and Mass Transfer 98 (2018) 223–231. `doi:10.1016/j.icheatmasstransfer.2018.09.011`.

[36] Z. Jiang, Z. Qu, Lithium–ion battery thermal management using heat pipe and phase change material during discharge–charge cycle: A comprehensive numerical study, Applied Energy 242 (2019) 378–392. `doi:10.1016/j.apenergy.2019.03.043`.

[37] A. Arshad, M. Jabbal, P. T. Sardari, M. A. Bashir, H. Faraji, Y. Yan, Transient simulation of finned heat sinks embedded with PCM for electronics cooling, Thermal Science and Engineering Progress 18 (2020) 100520. `doi:10.1016/j.tsep.2020.100520`.

[38] R. Y. Farsani, A. Raisi, A. A. Nadooshan, S. Vanapalli, Does nanoparticles dispersed in a phase change material improve melting characteristics?, International Communications in Heat and Mass Transfer 89 (2017) 219–229. `doi:10.1016/j.icheatmasstransfer.2017.10.006`.

[39] L. Colla, D. Ercole, L. Fedele, S. Mancin, O. Manca, S. Bobbo, Nano-phase change

materials for electronics cooling applications, Journal of Heat Transfer 139 (5). `doi:` `10.1115/1.4036017.`

[40] H. Faraji, M. Faraji, M. E. Alami, Numerical study of the transient melting of nano-enhanced phase change material, Heat Transfer Engineering (2019) 1–20`doi:10.1080/` `01457632.2019.1692496.`

[41] H. Faraji, M. Faraji, M. E. Alami, Numerical survey of the melting driven natural convection using generation heat source: Application to the passive cooling of electronics using nano-enhanced phase change material, Journal of Thermal Science and Engineering Applications 12 (2) (2020) 021005. `doi:10.1115/1.4044167.`

[42] N. S. Dhaidan, J. Khodadadi, T. A. Al-Hattab, S. M. Al-Mashat, Experimental and numerical investigation of melting of phase change material/nanoparticle suspensions in a square container subjected to a constant heat flux, International Journal of Heat and Mass Transfer 66 (2013) 672–683. `doi:10.1016/j.ijheatmasstransfer.2013.` `06.057.`

[43] J. M. Mahdi, E. C. Nsofor, Solidification of a PCM with nanoparticles in triplex-tube thermal energy storage system, Applied Thermal Engineering 108 (2016) 596–604. `doi:10.1016/j.applthermaleng.2016.07.130.`

[44] M. Ghalambaz, A. Doostani, A. J. Chamkha, M. A. Ismael, Melting of nanoparticles-enhanced phase-change materials in an enclosure: Effect of hybrid nanoparticles, International Journal of Mechanical Sciences 134 (2017) 85–97. `doi:10.1016/j.ijmecsci.` `2017.09.045.`

[45] A. Arshad, M. Jabbal, Y. Yan, Thermophysical characteristics and application of metallic-oxide based mono and hybrid nanocomposite phase change materials for thermal management systems, Applied Thermal Engineering 181 (2020) 115999. `doi:` `10.1016/j.applthermaleng.2020.115999.`

[46] A. Arshad, M. Jabbal, Y. Yan, Preparation and characteristics evaluation of mono and hybrid nano-enhanced phase change materials (NePCMs) for thermal management of microelectronics, Energy Conversion and Management 205 (2020) 112444. `doi:` `10.1016/j.enconman.2019.112444.`

[47] M. R. Safaei, H. R. Goshayeshi, I. Chaer, Solar still efficiency enhancement by using graphene oxide/paraffin nano-PCM, Energies 12 (10) (2019) 2002. `doi:10.3390/en12102002`.

[48] M. Sarafraz, M. Safaei, A. Leon, I. Tlili, T. Alkanhal, Z. Tian, M. Goodarzi, M. Arjomandi, Experimental investigation on thermal performance of a PV/t-PCM (photovoltaic/thermal) system cooling with a PCM and nanofluid, Energies 12 (13) (2019) 2572. `doi:10.3390/en12132572`.

[49] M. Alizadeh, K. Hosseinzadeh, D. Ganji, Investigating the effects of hybrid nanoparticles on solid-liquid phase change process in a y-shaped fin-assisted LHTESS by means of FEM, Journal of Molecular Liquids 287 (2019) 110931. `doi:10.1016/j.molliq.2019.110931`.

[50] K. Hosseinzadeh, M. Alizadeh, M. Alipour, B. Jafari, D. Ganji, Effect of nanoparticle shape factor and snowflake crystal structure on discharging acceleration LHTESS containing (al2o3-GO) HNEPCM, Journal of Molecular Liquids 289 (2019) 111140. `doi:10.1016/j.molliq.2019.111140`.

[51] H. Faraji, M. E. Alami, A. Arshad, Investigating the effect of single and hybrid nanoparticles on melting of phase change material in a rectangular enclosure with finite heat source, International Journal of Energy Research 45 (2020) 4314 4330. `doi:10.1002/er.6095`.

[52] M. J. Ashraf, H. M. Ali, H. Usman, A. Arshad, Experimental passive electronics cooling: Parametric investigation of pin-fin geometries and efficient phase change materials, International Journal of Heat and Mass Transfer 115 (2017) 251–263. `doi:10.1016/j.ijheatmasstransfer.2017.07.114`.

[53] Pcm rt-line, rt28hc, rubitherm technologies gmbh, accessed: 18/03/2021.
URL `https://www.rubitherm.eu/en/index.php/productcategory/organische-pcm-rt`

[54] M. Eisapour, A. H. Eisapour, M. Hosseini, P. Talebizadehsardari, Exergy and energy analysis of wavy tubes photovoltaic-thermal systems using microencapsulated PCM nano-slurry coolant fluid, Applied Energy 266 (2020) 114849. `doi:10.1016/j.apenergy.2020.114849`.

[55] H. Eshgarf, R. Kalbasi, A. Maleki, M. S. Shadloo, A. karimipour, A review on the properties, preparation, models and stability of hybrid nanofluids to optimize energy consumption, Journal of Thermal Analysis and Calorimetry (2020) 1–25 `doi:10.1007/s10973-020-09998-w`.

[56] B. Leonard, A stable and accurate convective modelling procedure based on quadratic upstream interpolation, Computer Methods in Applied Mechanics and Engineering 19 (1) (1979) 59–98. `doi:10.1016/0045-7825(79)90034-3`.

[57] S. Patankar, Numerical heat transfer and fluid flow, Hemisphere Publishing Corporation; McGraw-Hill Book Company, New York., 2018.

[58] J. M. Mahdi, E. C. Nsofor, Melting enhancement in triplex-tube latent thermal energy storage system using nanoparticles-fins combination, International Journal of Heat and Mass Transfer 109 (2017) 417–427. `doi:10.1016/j.ijheatmasstransfer.2017.02.016`.